The electrodiffusional theory for the wall shear stress measurement by two-strip probe

Vaclav Harrandt, David Kramolis, Florian Huchet, Jaroslav Tihon, Jaromir Havlica

The electro-diffusional theory for the wall shear stress measurement by two-strip probes

Vaclav Harrandt[a,b], David Kramolis[b], Florian Huchet[c], Jaroslav Tihon[a], Jaromir Havlica[a,b,*]

[a] *The Czech Academy of Sciences, Institute of Chemical Process Fundamentals, Rozvojova 2/135, 165 02 Prague, Czech Republic*
[b] *Jan Evangelista Purkyně University in Ústí nad Labem, Faculty of Science, Pasteurova 3632/15, 400 96 Ústí nad Labem, Czech Republic*
[c] *Univ. Gustave Eiffel, MAST-GPEM, Fr-44344 Bouguenais, France*

Abstract

This article deals with the derivation of a fundamental theory for describing mass transport on the active surface of a two-strip mass transfer probe for an arbitrary direction of the fluid flow. The existence and finding of such a general theory is a critical point for using the electrodiffusion method by employing two-strip probes. Considering changeable probe geometry, the general analytical formulas for the average mass transfer coefficients are derived and provided for both the probe segments in dimensionless forms . The correctness of the derived analytical expressions is confirmed by numerical solutions of the convection-diffusion transport equation.

Also, a methodology of possible experimental data treatment is proposed. It is based on the evaluation of two current signals collected from the segments of a two-strip probe. From the derived equations, it is possible to determine the magnitude and direction of the wall shear rate for both, predominantly frontal and also reversal flows. Established on the analysis of the current ratio predictions for various probe geometries, an optimal probe configuration is found out with respect to the sensitivity of flow direction measurement.

Keywords: Concentration boundary layer, Electrochemical method,

*Corresponding author
Email address: havlica@icpf.cas.cz (Jaromir Havlica)

Convective mass transfer, Wall shear rate, Two-strip probe

1. Introduction

Transport phenomena occurring in boundary layers are, to a significant extent, dependent on the course of wall shear stress [1]. Therefore, knowledge of the velocity gradient at the wall is strategic information to assess the local skin friction between the wall and the flowing fluid. In general, the importance of this interaction on the overall behavior of the system grows as the specific surface area increases. For this reason, it is necessary to deal seriously with contact between wall and fluid, especially in microfluidic devices [2], porous structures [3], or reactors containing packed beds [4] or structured layers [5].

Recently, an extraordinary expansion of microfluidics to fulfill the demands of process engineering or biomedical applications can be observed [6]. The requirements for wall shear stresses in these microflow devices differ and depend on the specific application. In the chemical industry, within these microdevices, it is often required to intensify transport phenomena and thus achieve a high magnitude of wall shear stresses [7]. On the other hand, in biomedicine or biotechnology, in devices applied for the cultivation of biological materials bonding on the wall, there is an effort to minimize wall shear stresses or at least not exceed the limit values [8]. Even if it is necessary to maximize wall shear stresses or vice versa, the fluid must behave respectfully towards the living organisms located on the device's wall; it is always essential to have information about the values of the velocity gradient on the wall.

However, direct measurement of wall shear stress is a complex challenge up to the present day. The reason is the need to describe hydrodynamics in the immediate vicinity of the wall, where conventional approaches usually fail because they cause disturbances in the flow structure. Therefore, for appropriate evaluation of wall shear stress, one needs to use noninvasive methods that do not significantly influence the flow structures and are applicable to locations situated on the wall [9]. In particular, the ability to evaluate flow information

close to the wall is a major limitation of most recently developing methods such as Particle Image Velocimetry (PIV) [10] or Laser-Induced Fluorescence (LIF) [11]. Although these optical non-intrusive methods highly accurately describe hydrodynamics even in complex geometries, they still cannot adequately capture phenomena occurring directly at the wall.

One possible technique for the nonintrusive measurement of wall shear stress is the electro-diffusion (ED) method, which can be recently viewed as a possible adept for near-wall flow diagnostics in microfluidic devices [12]. This method was initially introduced by Reiss & Hanratty [13] for measuring instantaneous rates of mass transfer to a small wall probe. This technique was afterward applied also to measure the velocity gradient at the wall [14]. The principle of the ED method is based on the measurement of limiting electric current passing through a small electrode flush-mounted into the wall, and thus it is in many ways similar to that of hot wire anemometry. Nevertheless, instead of the temperature, the studied scalar quantity is the concentration of the active ions. As the involved electrochemical reaction is fast enough, the concentration of the reacting ions is zero at the electrode surface, and the measured current is fully controlled by convective-diffusive transport. When comparing the ED method to hot wire anemometry, the main advantage is in the absence of undesired loss of transported quantity [15]. A detailed description of the measuring principles can be found in several reviews [9, 15, 16, 17, 18].

The basic geometrical shapes of probes used for the ED method are circular, and strip [14]. Circular probes are intended just for the measurements of the magnitude of the wall shear rate [19]. As a separate measuring object, the single strip probe is though direction sensitive, but due to the need to determine two independent variables as are the magnitude and direction of the shear stress vector, it is unusable. Therefore, it is only appropriate for measuring shear stress magnitude for a strictly defined direction of fluid flow. This implies that if the direction of near-wall flow needs to be provided by the measurement, multi-segmented probes have to be applied. The so-called sandwich probes introduced by Son & Hanratty [20] is often used to detect a possible flow reversal in the near-

wall region. It consists of two strip segments separated by a thin insulating gap. In this case, the concentration boundary layer of the upstream (front) segment influences the mass transport on the downstream (rear) segment. By comparing the magnitudes of both current signals, it is possible to distinguish between the frontal and reversal direction of the flow [21]. In addition to evaluating shear rates in stationary flow, the ED method can also measure more complex flow types, such as unsteady oscillating flows. Mao & Hannratty [22, 23] developed the so-called inverse mass transfer method, which using numerical simulations and measured electrical current values, can adequately describe the frequency response of two-segmented probes for cases of oscillating flows [24, 25]. In the past, two-strip probes were used to measure wall shear rates and hydrodynamical description in many diverse applications. An example of the employment of a sandwich probes was the detection of stagnation and separation points in liquid flows around cylinders [20, 26], to recognize recirculation zones in the flow behind a backward-facing step [27], to detect the flow reversal under Taylor bubbles [28, 29], to investigate flow inside corrugated plate heat exchangers [30], or to determine the flow regimes in multiphase flows [31].

A more ingenious, three-segmented probe developed by Wein & Sobolík [32] is composed of three active parts having shapes of circular sectors. After specific directional calibration, this probe can measure instantaneous vectors of the wall shear rate. According to Lamarche-Gagnon & Vetel [33], similarly, as in the case of a two-segmented probe, the approach of the inverse method is applicable for oscillating flows also with the usage of a three-segmented probe. In general, however, the three-segmented probe has a problem with evaluating the stagnant point and is not entirely suitable for measuring high-frequency fluctuating flow.

To employ two-segmented probes for measurement using the ED method, it is necessary to have any connection in the form of an analytical equation between the measured currents from segments and the shear rate vector. This expression can be obtained by calibration or by theory. In the case of calibration, depending on the flow type, calibration equations describing the relations between electrical current and shear rate are used. The constants in these cali-

bration equations are subsequently evaluated using experimental measurements [34, 35]. The beginnings of the theoretical investigation of mass transfer on the surfaces of the two-strip probes were given by LeBouche [36]. For simplification, he used two equally long and wide segments and neglected the size of the insulating gap between them. Within the derived analytical relations framework connecting the measured currents from both segments and the wall shear rate, he assumed a perpendicular flow of the liquid through the transverse leading edge. The theory for evaluating measurements using two-strip probes was further broadened by Py [37]. The probe geometry and liquid flow angle were identical to those of LeBouche [36]. Unlike LeBouche, Py assumed the influence of the insulating gap, which he evaluated based on numerical simulations. The pinnacle of theoretical research for the evaluation of measured data for a two-strip probe can be considered the publication by the authors Wein & Wichterle [38] from 1989. They generalized the theory for a two-strip probe for mutually different lengths of both segments, and also only, based on the theory, they deduced the influence of the thickness of the gap on mass transport on both segments. However, the question of generalization of this problem for arbitrary flow orientation remains unanswered to this day.

The existence and finding of such a general theory is a critical point for using the electrodiffusion method to measure both the magnitude of the shear rate vector and the flow direction by employing two-strip probes. Therefore, the presented work focuses on deriving a fundamental theory for describing mass transport for an arbitrary fluid flow direction with a constant velocity gradient for two-strip mass transfer probes. This work follows our previous publication [1], in which we revisited the electro-diffusional theory for the wall shear stress measurement from single mass transfer probes of rectangular shape by considering the existence of two components of the wall shear rate (i.e., longitudinal and transversal). The published theory was generalized to the two-strip probes in the present paper. The correctness of the derived analytical relations for arbitrary flow direction and the aspect ratio of both segments was confirmed by numerical solutions of the transport equation in the convective-diffusive regime.

Finally, we presented both the new measurement methodology with a two-strip probe concerning the longitudinal and transversal flow directions and requirements for the optimal geometrical configuration measurement probe. Based on our research and theory, the possibility opens up to apply a two-strip probe not only for flow reversal detection but also to determine the actual flow direction.

2. Theory of wall shear stress measurements by two-strip probe

2.1. Principle of limiting diffusion current measurements

An electrodiffusion method measures instantaneous local mass transfer rates on the surface of an electrode, where a rapid redox reaction takes place. When a sufficiently high polarization voltage is applied to the electrochemical system, the concentration of reacting species on the electrode is zero, and the limiting current flowing through the created electrochemical cell is controlled only by the mass transfer of reacting species towards the electrode. Therefore, based on the value of the measured current, the mass transfer coefficient, and subsequently also, the wall shear rate can be determined. The relationship between the measured current signal and the wall shear rate can be ascertained either by a reliable calibration method or by finding adequate analytical formulas.

Calibration, as the first possibility, is generally suitable for circular electrodes because their symmetrical shape is not sensitive to the flow direction. In such a case, only the current dependence on the magnitude of the shear rate vector is solved. However, for strip and segmented probes, the use of calibration is very limited due to the dependence of the measured current not only on the magnitude of the shear rate vector but also on the flow direction. Another limiting factor for performing calibration is the usually fixed position of probes with respect to the wall of an experimental device and, thus, limited possibilities for controlling the flow direction in a defined manner during calibration.

Utilization of analytical expressions, as the second possibility how to solve this problem, requires the existence of a unified theory relating both quantities. However, due to the complicated transport phenomena on the electrode's sur-

face, finding the exact relation valid for an arbitrary flow direction is problematic, especially for segmented electrodes. But still, solving this task is necessary to make direction-sensitive measurements with segmented probes possible.

The governing equation that links the experimental measurement of the limiting current I_{lim} to the mass transport to the electrode surface is Faraday's law of electrolysis, which is expressed as

$$I_{\mathrm{lim}} = |\overline{J}_z| n_{\mathrm{e}} S_{\mathrm{e}} F \,, \tag{1}$$

where $\overline{J}_z$ denotes the molar flux intensity in z-direction, n_{e} is the number of electrons involved in the redox reaction, S_{e} indicates the size of the active surface area of the electrode, and F is the Faraday constant. The average intensity of the flow of ions to the surface of the electrode can be expressed as

$$\overline{J}_z = -\overline{k}_z (c_\infty - c_{\mathrm{w}}) \,, \tag{2}$$

where c_∞ is bulk concentration, c_{w} is equilibrium concentration on the probe surface, and the proportionality constant is represented by the average mass transfer coefficient $\overline{k}_z$ which is taking into account mass flow through both diffusion and convective mechanisms in z-direction. The concentration difference in the equation (2) is the driving force of the ongoing mass transport.

From Faraday's law, eq. (1), the mass transfer coefficient can be calculated based on the measured electric current, which forms a kind of entrance gate for determining the investigated hydrodynamic quantities near the wall. However, to bridge the gap between the mass transfer coefficient and the studied quantities, it is necessary to use suitable relations based on a theory that is approached and derived in the following text.

2.2. Analytical solution for a single strip probe

The investigated situation is shown schematically in Fig. 1. The probe dimensions are defined using its longitudinal length L_x in the direction of the x-axis and its transverse width L_y in the direction of the y-axis, see Fig. 1. Also, to provide and analyze the results obtained for different strip configurations,

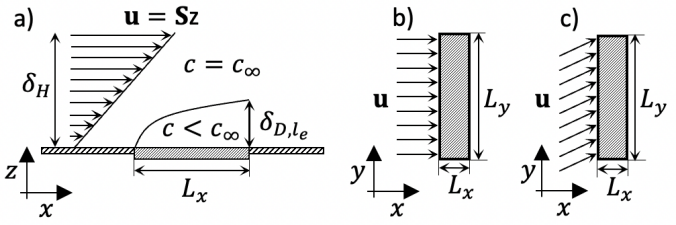

Figure 1: Scheme of the investigated system with a single strip probe: a) flow and mass transfer in the near-wall region of the strip probe in xz plane; b) perpendicular fluid flow over probe surface in xy plane; c) arbitrary direction fluid flow over probe surface in xy plane.

the probe width L_y is permanently fixed, whereas only the probe length L_x is changed.

When describing hydrodynamics near the probe surface, a simple shear flow with an arbitrary angle α concerning the x-axis is assumed. The angle α is thus defined as the arctangent of the ratio of the transverse velocity component u_y to the longitudinal one u_x. For the homogeneous simple shear flow, the angle α is connected with the components of the wall shear rate vector $\mathbf{S}$. Therefore, it is convenient to introduce the non-dimensional parameter β defined as

$$\beta = \frac{S_y^2}{\|\mathbf{S}\|^2} = \cos^2\alpha\,, \quad 1-\beta = \frac{S_x^2}{\|\mathbf{S}\|^2} = \sin^2\alpha\,, \tag{3}$$

where S_x and S_y are components of the wall shear rate vector, and $\|\mathbf{S}\|$ is its magnitude. The dimensionless angle takes the values $\beta \in \langle 0, 1\rangle$ corresponding to the angle $\alpha \in \langle 0, \pi/2\rangle$. This interval is determined by the nature of the strip probe, which exhibits certain symmetry concerning the flow direction, thus giving outside this interval ($\alpha < 0$ or $\alpha > \pi/2$) identical results as inside this interval ($\overline{k}_z(\alpha) \equiv \overline{k}_z(-\alpha)$ and for $\overline{k}_z(\alpha) \equiv \overline{k}_z(\pi - \alpha)$), see Fig. 2.

For the definition of the mass transfer coefficient, the so-called critical value of the β parameter is of specific importance. It indicates the size of the dimensionless angle in such a configuration of the system in which the ratio of the lengths of the probe's sides is equal to the ratio of the longitudinal and

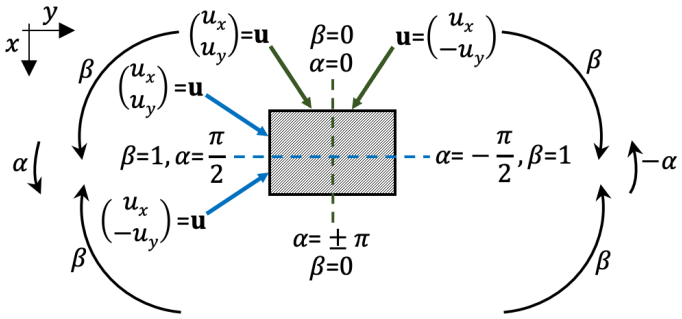

Figure 2: Scheme of strip probe: (i) two types of the measuring symmetry for evaluation of the fluid flow angle; the axis of the first symmetry is the green dashed line, and the axis of the second symmetry is the blue dashed line; (ii) the relation between the dimensionless angle β and the angle α.

transverse components of the velocity vector

$$\frac{L_x}{L_y} = \frac{u_x}{u_y} = \frac{\sqrt{1-\beta_c}}{\sqrt{\beta_c}} \Rightarrow \beta_c = \frac{L_y^2}{L_x^2 + L_y^2} = \frac{1}{R^2+1}\,. \tag{4}$$

The geometrical parameter R is the aspect ratio between the length and width of the rectangular probe

$$R = \frac{L_x}{L_y}\,. \tag{5}$$

The description of mass transport in the vicinity of the probe is described by governing equation

$$\frac{\partial c}{\partial t} + u_x\frac{\partial c}{\partial x} + u_y\frac{\partial c}{\partial y} + u_z\frac{\partial c}{\partial z} = D\left(\frac{\partial^2 c}{\partial x^2} + \frac{\partial^2 c}{\partial y^2} + \frac{\partial^2 c}{\partial z^2}\right)\,, \tag{6}$$

where t is time, c is concentration, D is diffusion coefficient and u_x, u_y, u_z are the components of the velocity field vector. It is considered that the flow is homogeneous over the surface of the probe without any stagnation points ($u_z \approx 0$). The concentration profile is steady, ($\partial c/\partial t = 0$). The Schmidt number, defined as the ratio of kinematic viscosity, ν, and diffusion coefficient, D,

$$Sc = \frac{\nu}{D}\,, \tag{7}$$

is sufficiently large, and therefore, the components of the velocity vector (u_x, u_y) change only in the normal direction to the electrode surface as a linear function

in the viscous sublayer

$$u_x = S_x z = \frac{\partial u_x}{\partial z} z\,; \quad u_y = S_y z = \frac{\partial u_y}{\partial z} z\,. \tag{8}$$

If the Peclet numbers, represented as the ratio of the product of the characteristic length and the characteristic velocity to the diffusion coefficient,

$$Pe_x = \frac{L_x u_x}{D}\,; \quad Pe_y = \frac{L_y u_y}{D}\,, \tag{9}$$

is also sufficiently large, convective transport dominates over diffusion

$$D\left(\frac{\partial^2 c}{\partial x^2}\right) \approx 0\,, \quad D\left(\frac{\partial^2 c}{\partial y^2}\right) \approx 0\,. \tag{10}$$

By combining all the above assumptions (discussed in more depth in the publication of Havlica et al. [1]), the equation (6) takes the form

$$S_x z \frac{\partial c}{\partial x} + S_y z \frac{\partial c}{\partial y} = D \frac{\partial^2 c}{\partial z^2}\,. \tag{11}$$

The equation (11) suggests that the mass transport in the direction of the x- and y-axes is ensured by convection, while in the direction of the z-axis only by diffusion. Therefore, the mean integral value of the molar flow intensity in the normal direction, $\overline{J}_z$, over the whole probe surface is given by using Fick's law

$$\overline{J}_z = \frac{1}{S}\int_S J_z \mathrm{d}S = \frac{1}{S}\int_S \left(-D\frac{\partial c}{\partial z}\right)_{z=0} \mathrm{d}S\,. \tag{12}$$

Combining the equations (2) and (12), the formula for the average mass transfer coefficient is defined as

$$\overline{k}_z = \frac{1}{(c_\infty - c_\mathrm{w})S}\int_S \left(D\frac{\partial c}{\partial z}\right)_{z=0} \mathrm{d}S\,. \tag{13}$$

To describe mass transport in the close vicinity of the strip probe, it is necessary to solve the partial differential equation (11). But, unfortunately, in the case of arbitrary flow direction, the given differential equation cannot be solved analytically in general. For this reason, it is necessary to propose a different procedure, which consists of the following two steps: (i) performing a geometric transformation of the measuring probe so that the average mass

transfer coefficient for the situation of the arbitrary flow direction was identical to the average mass transfer coefficient for the transformed probe with the perpendicular flow; (ii) finding a mass transport solution for the perpendicular flow of fluid over the newly transformed probe. This transformation makes it possible to obtain an analytical solution for the arbitrary flow direction.

For the case of perpendicular fluid flow with respect to the leading edge of the probe ($u_y = 0$, see Fig.1b), the transport equation (11) is simplified to the form

$$S_x z \frac{\partial c}{\partial x} = D \frac{\partial^2 c}{\partial z^2}\,, \tag{14}$$

with the following boundary conditions

$$\begin{array}{ccc} x \to -\infty & z > 0 & c = c_\infty \\ x \in \langle 0, L_x \rangle & z = 0 & c = c_\mathrm{w} \\ x < 0 \cup x > L_x & z = 0 & \partial c/\partial z = 0 \\ x \to \infty & z > 0 & \partial c/\partial x = 0 \\ \forall x & z \to \infty & c = c_\infty \end{array}\,. \tag{15}$$

The analytical solution of the above second-order partial differential equation can be expressed in the shape [14]

$$\frac{c - c_\mathrm{w}}{c_\infty - c_\mathrm{w}} = \frac{1}{\Gamma(\frac{4}{3})} \int_0^\eta e^{-\eta^3} \mathrm{d}\eta\,, \tag{16}$$

where Γ is the gamma function. The variable η is determined by the prescription

$$\eta = z \left(\frac{S_x}{9xD} \right)^{\frac{1}{3}}\,. \tag{17}$$

The mass transfer coefficient on the surface of the probe is a function of the x-coordinate only, and the equation (13) reduces to the expression

$$\overline{k}_z = \frac{1}{(c_\infty - c_\mathrm{w}) L_x} \int_0^{L_x} \left(D \frac{\partial c}{\partial z} \right) \mathrm{d}x\,. \tag{18}$$

By derivative of the concentration field described in the equation (16) according to the z-coordinate and subsequent integration, the following equation is obtained

$$\overline{k}_z = \frac{3}{2\Gamma(\frac{4}{3}) 9^{\frac{1}{3}}} \left(\frac{D^2 S_x}{L_x} \right)^{\frac{1}{3}} = K_\mathrm{L} \left(\frac{D^2 S_x}{L_x} \right)^{\frac{1}{3}}\,, \tag{19}$$

where K_{L} is Lévêque constant

$$K_{\mathrm{L}} \doteq 0.807549\,. \tag{20}$$

A detailed derivation of the Eq. (19) is reported in Appendix A. According to the Eq. (19), the average mass transfer coefficient is dependent on the diffusion coefficient, D, the length of the strip probe, L_x, and the x-component of wall shear rate vector, S_x.

The normalized Sherwood number as a nondimensional form of the average mass transfer coefficient is then defined as

$$Sh^*_{L_x} = \frac{\overline{k}_z \delta_{D,L_x}}{D} = \overline{k}_z \left(\frac{L_x}{D^2 S_x} \right)^{\frac{1}{3}} = K_{\mathrm{L}}\,, \tag{21}$$

where δ_{D,L_x} is the thickness of the diffusion boundary layer, and according to Guyon [39], scaling for this thickness can be written in the form

$$\delta_{D,L_x} \approx \left(\frac{D L_x}{\|\mathbf{S}\|} \right)^{\frac{1}{3}}\,. \tag{22}$$

In the case of perpendicular flow over the leading edge of the strip probe, it is possible to relate the average mass transfer coefficient unambiguously to the scalar value of the wall shear rate and Eq. (21) became the basis of the electrodiffusion method described in publications by Reiss & Hanratty [13, 14].

Now, to solve the case of an arbitrary flow (see Fig.1c), the above-mentioned geometric transformation of the probe has to be applied. The basic idea of this transformation is to divide the probe into individual sub-sections of infinitesimal widths oriented in the flow direction. Each sub-section will be viewed as a separate rectangular probe of length $l(v)$ and width $\mathrm{d}v$ subjected to the perpendicular flow. In this case, the local mass transfer coefficient can be written based on the equation (19) as

$$k_z = K_{\mathrm{L}} \left(\frac{D^2 \|\mathbf{S}\|}{l(v)} \right)^{\frac{1}{3}}\,. \tag{23}$$

The average value of the mass transfer coefficient can be obtained by integrating k_z over the active surface of the probe

$$\overline{k}_z = \frac{1}{S} \int_S k_z \mathrm{d}S = \frac{1}{L_x L_y} \int_v k_z l(v) \mathrm{d}v\,, \tag{24}$$

where $\mathrm{d}S = l(v)\mathrm{d}v$, and active surface of a probe is defined as $S = L_x L_y$. By subsequently substituting the Eq. (23) into the Eq. (24), one can obtain

$$\overline{k}_z = \frac{K_\mathrm{L}}{L_x L_y}(D^2\|\mathbf{S}\|)^{\frac{1}{3}} \int_v l(v)^{\frac{2}{3}}\mathrm{d}v\,. \tag{25}$$

The equation (25) can be rewritten in an analogous form as Eq. (23)

$$\overline{k}_z = K_\mathrm{L}\left(\frac{D^2\|\mathbf{S}\|}{l_\mathrm{e}}\right)^{\frac{1}{3}}, \tag{26}$$

where

$$l_\mathrm{e} = \left(\frac{L_x L_y}{\int_v l(v)^{\frac{2}{3}}\mathrm{d}v}\right)^3. \tag{27}$$

The quantity l_e represents effective transfer length. The mathematical expression of the integral $\int_v l(v)^{2/3}\mathrm{d}v$ and, in detail, the whole process for deriving the mass transfer coefficient and the normalized Sherwood number for a strip probe and the arbitrary direction of simple shear flow can be found in the publication of Havlica et al.[1].

The effective transfer length is a function of the dimensionless angle, β, the geometrical aspect ratio of the strip probe, R, and the probe length, L_x, and it is defined as [1]

$$l_\mathrm{e}^{\frac{1}{3}} = \begin{cases} \dfrac{L_x^{\frac{1}{3}}}{(1-\beta)^{\frac{1}{6}}\left(1+\dfrac{R\sqrt{\beta}}{5\sqrt{1-\beta}}\right)} & \text{for} \quad \beta \le \beta_\mathrm{c} \\ \dfrac{L_x^{\frac{1}{3}}}{\beta^{\frac{1}{6}}R^{\frac{1}{3}}\left(1+\dfrac{\sqrt{1-\beta}}{5R\sqrt{\beta}}\right)} & \text{for} \quad \beta > \beta_\mathrm{c} \end{cases}. \tag{28}$$

The effective transfer length is a length that corresponds to the longitudinal length of an apparent rectangular probe exposed to the perpendicular liquid flow, which has the same average mass transfer coefficient as the real measuring probe exposed to an arbitrary flow direction.

To characterize mass transport on the active surface of a strip probe, it is convenient to use the dimensionless form of average mass transfer coefficient in the form of a normalized Sherwood number. The general expression for the

normalized Sherwood number for any 2D fluid flow over the probe surface is defined in our previous work [1] as

$$Sh^*_{l_D} = \frac{\overline{k}_z \delta_{D,l_D}}{D} = K_{\mathrm{L}} \left(\frac{l_D}{l_{\mathrm{e}}} \right)^{\frac{1}{3}} , \tag{29}$$

where

$$\delta_{D,l_D} = \left(\frac{D l_D}{\|\mathbf{S}\|} \right)^{\frac{1}{3}} . \tag{30}$$

The characteristic length l_D determines the thickness of the diffusion boundary layer, δ_{D,l_D}. In the following text, two characteristic lengths are used to define the normalized Sherwood number. The first one is the effective transfer length, l_{e}, and the second one is the probe length L_x. In the first case, the equation (29) reduces to the form

$$Sh^*_{l_{\mathrm{e}}} = K_{\mathrm{L}} \, . \tag{31}$$

In the second case, the normalized Sherwood number has the form

$$Sh^*_{L_x} = \frac{\overline{k}_z \delta_{D,L_x}}{D} = K_{\mathrm{L}} \left(\frac{L_x}{l_{\mathrm{e}}} \right)^{\frac{1}{3}} . \tag{32}$$

2.3. Analytical solution for a two-strip probe

Havlica et al. [1] proposed an electro-diffusional measurement methodology using two single-strip probes to obtain both, the magnitude of wall shear rate and the near-wall flow direction. The most problematic point of the proposed method is that during the experiment, it must be guaranteed that the changes in the concentration fields due to the electrochemical reactions on both probes do not mutually interfere with each other. This requirement can be fulfilled either by a sufficient probe separation or by a suitable measurement timing. However, both these options are very limiting for local measurements of near-wall flow structures. Therefore, it is necessary to establish a new fundamental theory that considers the interaction of the adjacent measuring probes and thus allows the simultaneous measurement of both the magnitude and direction of the near-wall flow. For this reason, in this section, necessary formulas describing mass transport on the surface of two-segmented strip probes in a sandwich

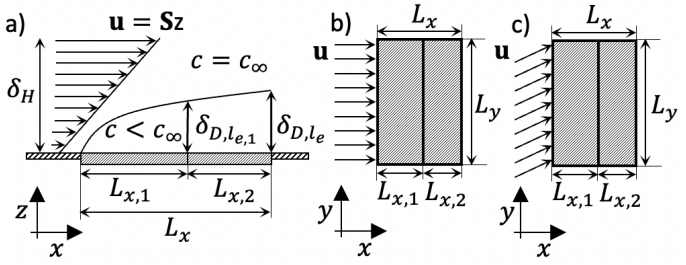

Figure 3: Scheme of the investigated system of two segmented strip mass transfer probes: a) flow and mass transfer in the near-wall region of the strip probes in xz plane; b) perpendicular fluid flow over probe surfaces in xy plane; c) arbitrary direction fluid flow over probes surface in xy plane.

arrangement are derived for the case of simple shear flow with an arbitrary direction. In deriving the given theory, an idealization assumption is introduced, supposing that even though the measuring probes are in direct contact, they are electrically isolated from each other. Since manufacturing capabilities allow insulation thicknesses on the order of micrometers [29], this idealization does not cause too much distortion of reality. However, the effect of the gap between the probes will be the subject of further research.

The discussed system is illustrated in figure 3a. For simplification, the following analysis of mass transport on the two-strip probe surface is divided into two parts. The first case assumes the perpendicular flow over the leading edge of the probe (figure 3b). The second case considers the arbitrary direction of flow over the leading probe edge (figure 3c). The first case leads to the Wein & Wichterle analytical solution [38]. The second part presents the generalized analytical solution of mass transport for two-strip probes for the arbitrary direction of simple shear flow, which has not been reported yet.

The following discussion on the two-strip probe is distinguished the mass transport at the front and rear segments and at the merged probe. The front segment is not affected by the concentration boundary layer of the rear one, and it behaves independently as a single probe. The solution of mass transport on the front segment was described in the publication of Havlica et al. [1]. On the

other hand, the rear probe is, in most cases, in the concentration wake caused by the electrochemical reaction taking place on the front segment. Therefore, mass transport on the rear segment is significantly affected by the thickness of the diffusion boundary layer created due to ongoing transport phenomena on the front segment. The merged probe is created by connecting the front and rear segments to one. The merged probe behaves independently in the same way as the single probe. The quantities associated with the front segment are marked with subscript index 1, the quantities connected with the rear segment with subscript index 2, and the merged probe quantities are without an index describing the electrode.

2.3.1. The case of perpendicular flow direction

The mass transfer coefficients of the two-strip probe in a sandwich arrangement are first derived for the case of perpendicular flow direction (see Fig. 3b). To define the probe geometry, the lengths L_{x1} and L_{x2} of the individual measuring probes are bound by the following equalities

$$L_{x1} = aL_x\,, \quad L_{x2} = (1-a)L_x\,, \tag{33}$$

where

$$a \in \langle 0\,;1\rangle\,. \tag{34}$$

The variable a is the dividing coefficient, and the borderline cases $a = 0$ and $a = 1$ correspond to scenarios where there is only one measuring probe with dimensions $L_x \times L_y$ in the studied system. In the case of a two-strip probe, it is necessary also define the geometrical parameters R_1, and R_2 as the ratios of the length and width of the rectangular front and rear segments

$$R_1 = \frac{aL_x}{L_y} = \frac{L_{x1}}{L_{y1}}\,, \tag{35}$$

$$R_2 = \frac{(1-a)L_x}{L_y} = \frac{L_{x2}}{L_{y2}}\,. \tag{36}$$

The equations for the z-component of the molar flow intensities can be for individual segments obtained by using the equation (12), in which the areas of

partial electrodes are taken into account in the integration limits

$$\overline{J}_{z1} = \frac{1}{aL_x} \int_0^{aL_x} \left(D \frac{\partial c}{\partial z} \right)_{z=0} \mathrm{d}x \,, \tag{37}$$

$$\overline{J}_{z2} = \frac{1}{(1-a)L_x} \int_{aL_x}^{L_x} \left(D \frac{\partial c}{\partial z} \right)_{z=0} \mathrm{d}x \,. \tag{38}$$

Established on the derivation procedure given for the single probe in Appendix A, the values of the average mass transfer coefficients on the active surface of each segment can be assessed from the knowledge of the concentration field described by Eq. (16)

$$\overline{k}_{z1} = \frac{1}{\Gamma(\frac{4}{3})} \frac{1}{aL_x} \left(\frac{D^2 S_x}{9} \right)^{\frac{1}{3}} \int_0^{aL_x} x^{-\frac{1}{3}} \mathrm{d}x \,, \tag{39}$$

$$\overline{k}_{z2} = \frac{1}{\Gamma(\frac{4}{3})} \frac{1}{(1-a)L_x} \left(\frac{D^2 S_x}{9} \right)^{\frac{1}{3}} \int_{aL_x}^{L_x} x^{-\frac{1}{3}} \mathrm{d}x \,. \tag{40}$$

By solving the integral in Eqs. (39) and (40) and by subsequent simple adjustments, the following relations can be obtained

$$\overline{k}_{z1} = K_{\mathrm{L}} \frac{1}{a^{\frac{1}{3}}} \left(\frac{D^2 S_x}{L_x} \right)^{\frac{1}{3}} \,, \tag{41}$$

$$\overline{k}_{z2} = K_{\mathrm{L}} \frac{1-a^{\frac{2}{3}}}{1-a} \left(\frac{D^2 S_x}{L_x} \right)^{\frac{1}{3}} \,. \tag{42}$$

The dimensionless forms of the average mass transfer coefficient expressed using the normalized Sherwood number can then be written as

$$Sh^*_{1,L_{x1}} = Sh^*_{L_x} = \frac{\overline{k}_{z1} \delta_{D,L_{x1}}}{D} = K_{\mathrm{L}} \,, \tag{43}$$

$$Sh^*_{2,L_x} = \frac{\overline{k}_{z2} \delta_{D,L_x}}{D} = K_{\mathrm{L}} \frac{1-a^{\frac{2}{3}}}{1-a} \,. \tag{44}$$

For the front segment, the thickness of the diffusion boundary layer is evaluated at the length L_{x1}. However, the diffusion boundary layer built at the rear segment is already affected by mass transport at the front one. Therefore, the characteristic length controlling the thickness of its boundary layer is equal to the length of the merged probe L_x. The front segment behaves independently and acquires the identical value of Sh^* as the single probe, compare Eqs. (21)

and (43). On the other hand, the rear segment exhibits less intense mass transfer with the magnitude of normalized Sherwood number already depending on the dividing coefficient a.

The ratios of electrical currents, average mass transfer coefficients, and normalized Sherwood numbers relate the quantities corresponding to the rear and front segments of the two-strip probe. The expression for the ratio of currents is obtained by combining Eqs. (1), (2), (41), and (42)

$$\frac{I_2}{I_1} = a^{-\frac{2}{3}} - 1\,, \tag{45}$$

the expression for the ratio of average mass transfer coefficients by combining Eqs. (41), and (42)

$$\frac{\overline{k}_{z2}}{\overline{k}_{z1}} = \frac{a^{\frac{1}{3}} - a}{1 - a}\,, \tag{46}$$

and finally, the expression for the ratio of normalized Sherwood numbers by combining Eqs. (43), and (44)

$$\frac{Sh^*_{2,L_x}}{Sh^*_{1,L_{x1}}} = \frac{1 - a^{\frac{2}{3}}}{1 - a}\,. \tag{47}$$

The dependence of these ratios on the value of dividing coefficient a is plotted in Fig. 4.

The current ratio I_2/I_1 exhibits a decreasing dependence on the dividing coefficient a, see Fig. 4a). As the dividing coefficient a is increased, the area of the front segment and thus also mass transport taking place there increases at the expense of the rear segment area. The magnitudes of electric currents flowing through both the probe segments become identical for the value of dividing coefficient $a = 2^{-3/2}$, i.e., approximately the first one-third of merged probe area, $L_x \times L_y$, provides the same electric current as the remaining two-thirds of merged probe area. Obviously, for two limiting cases, it holds: $a \to 0$ (negligible front segment), $I_2/I_1 \to \infty$ and $a \to 1$ (negligible rear segment), $I_2/I_1 \to 0$. The derived dependence described by Eq. (45) agrees precisely with the solution derived by Wein & Wichterle [38].

As the average mass transfer coefficients and normalized Sherwood numbers are not cumulative quantities but those are averaged over the probe surface, the

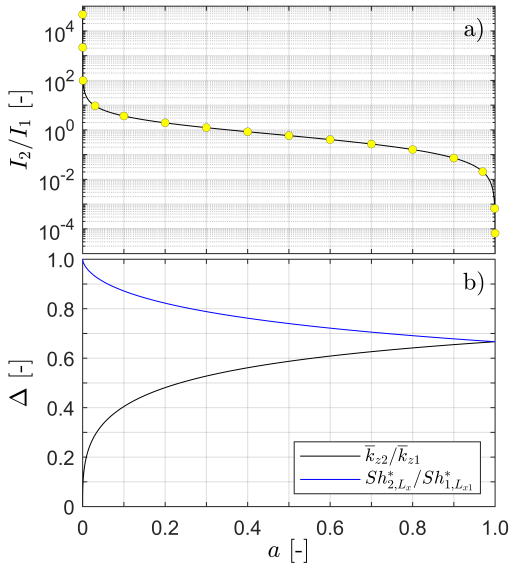

Figure 4: The dependence of the ratio of essential variables characterizing the rear and the front electrodes for the case of the perpendicular flow over the leading edge of the two-segmented probe on the dividing coefficient a: a) the ratio of electric currents flowing through the electrodes, I_2/I_1, derived on the base of our theory; b) the mass transfer coefficients $\Delta \equiv \overline{k}_{z2}/\overline{k}_{z1}$, and the normalized Sherwood numbers $\Delta \equiv Sh^*_{2,L_x}/Sh^*_{1,L_{x1}}$ derived on the base of our theory.

ratios of these quantities follow somewhat different trends when the dividing coefficient a is increased (see Fig. 4b). As the maximum value of the average mass transfer coefficient is observed at the leading edge of the probe, the average mass transfer coefficients for both probe segments are decreased when the value of the dividing coefficient a is increased. But the more pronounced reduction is observed for the front segment. Therefore, the ratio of average mass transfer coefficients defined by Eq. (46) increases with increasing dividing coefficient a. Two limiting cases are determined based on Eq. (46) as: $a \to 0$, $\overline{k}_{z2}/\overline{k}_{z1} \to 0$ (for $\overline{k}_{z1} \to \infty$) and $a \to 1$, $\overline{k}_{z2}/\overline{k}_{z1} \to 2/3$.

The value of $Sh^*_{1,L_{x1}}$ according to equation (43) is only constant and is therefore independent of the parameter a. The variable Sh^*_{2,L_x} decreases with increasing a due to the decrease in the average mass transfer coefficient at the

rear segment, see Eq. (44). Therefore, in contrast to the average mass transfer coefficients ratio, the dependence of the ratio of the normalized Sherwood numbers of the rear and front segments decreases with increasing dividing coefficient a, see Fig. 4b). Two limiting cases are now determined based on Eq. (47) as: $a \to 0$, $Sh^*_{2,L_x}/Sh^*_{1,L_{x1}} \to 1$ and $a \to 1$, $Sh^*_{2,L_x}/Sh^*_{1,L_{x1}} \to 2/3$.

2.3.2. The case of arbitrary flow direction

The traditional way how to obtain the value of the average mass transfer coefficient is either through the concentration field near the electrode surface, as was done in the case of a perpendicular flow of liquid over the leading edge, or the second alternative is to use a transformation using the effective transfer length. Unfortunately, the first traditional method cannot be used because the partial differential equation (11) describing the mass transport near the electrode surface does not have a general analytical solution. The second method, successfully used in deriving the theory for mass transport on a strip electrode with the arbitrary simple shear flow, could be theoretically used, but the resulting procedure would be very complicated when applied to a two-strip probe. Therefore, here proposes an alternative approach for determining the expression of the average mass transfer coefficient $\overline{k}_z$. It is established on the cumulative mass transfer property at the wall providing the measured electric current. This procedure thus utilizes the fact that the current passing through the merged probe equals the sum of the currents measured at its front and rear segments.

The average mass transfer coefficient in the equation (13) takes the following form for the merged probe

$$\overline{k}_z = \frac{1}{L_x L_y} \frac{\displaystyle\int_0^{L_x} \int_0^{L_y} \left(D \frac{\partial c}{\partial z} \right) \mathrm{d}y \, \mathrm{d}x}{c_\infty - c_\mathrm{w}} \,. \tag{48}$$

For the sake of generalization, it is suitable to work with a non-dimensional form of the average mass transfer coefficient. Therefore, the equation (48) is substituted into the definition relation for the normalized Sherwood number

(29)

$$Sh^*_{l_D} = \frac{\delta_{D,l_D}}{L_x L_y} \frac{\int_0^{L_x} \int_0^{L_y} \left(\frac{\partial c}{\partial z}\right) \mathrm{d}y \, \mathrm{d}x}{c_\infty - c_\mathrm{w}} \,. \tag{49}$$

The integral in Eq. (49) can be divided into two parts according to the geometry of two individual probe segments

$$Sh^*_{l_D} = \frac{\delta_{D,l_D}}{L_x L_y} \frac{\int_0^{aL_x} \int_0^{L_y} \left(\frac{\partial c}{\partial z}\right) \mathrm{d}y \, \mathrm{d}x + \int_{aL_x}^{L_x} \int_0^{L_y} \left(\frac{\partial c}{\partial z}\right) \mathrm{d}y \, \mathrm{d}x}{c_\infty - c_\mathrm{w}} \,. \tag{50}$$

The normalized Sherwood numbers for the front and rear probe segments can be expressed in a similar way

$$Sh^*_{1,l_{D1}} = \frac{\overline{k}_{z1} \delta_{D,l_{D1}}}{D} = \frac{\delta_{D,l_{D1}}}{aL_x L_y} \frac{\int_0^{aL_x} \int_0^{L_y} \left(\frac{\partial c}{\partial z}\right) \mathrm{d}y \, \mathrm{d}x}{c_\infty - c_\mathrm{w}} \,, \tag{51}$$

$$Sh^*_{2,l_{D2}} = \frac{\overline{k}_{z2} \delta_{D,l_{D2}}}{D} = \frac{\delta_{D,l_{D2}}}{(1-a)L_x L_y} \frac{\int_{aL_x}^{L_x} \int_0^{L_y} \left(\frac{\partial c}{\partial z}\right) \mathrm{d}y \, \mathrm{d}x}{c_\infty - c_\mathrm{w}} \,. \tag{52}$$

Equations (51) and (52) can be adjusted to the forms

$$\frac{1}{L_x L_y} \frac{\int_0^{aL_x} \int_0^{L_y} \left(\frac{\partial c}{\partial z}\right) \mathrm{d}y \, \mathrm{d}x}{c_\infty - c_\mathrm{w}} = \frac{a Sh^*_{1,l_{D1}}}{\delta_{D,l_{D1}}} \,, \tag{53}$$

$$\frac{1}{L_x L_y} \frac{\int_{aL_x}^{L_x} \int_0^{L_y} \left(\frac{\partial c}{\partial z}\right) \mathrm{d}y \, \mathrm{d}x}{c_\infty - c_\mathrm{w}} = \frac{(1-a) Sh^*_{2,l_{D2}}}{\delta_{D,l_{D2}}} \,. \tag{54}$$

By combining the equations (53) and (54) with the equation (50), the relationship between these three normalized Sherwood numbers can be obtained

$$Sh^*_{l_D} = \delta_{D,l_D} \left[\frac{a Sh^*_{1,l_{D1}}}{\delta_{D,l_{D1}}} + \frac{(1-a) Sh^*_{2,l_{D2}}}{\delta_{D,l_{D2}}} \right] , \tag{55}$$

Since the merged probe and its front segment behave independently, and their behavior is not affected by another probe in the system, the value of the normalized Sherwood number of the merged probe is defined by the Eq. (29). For the front segment, the Eq. (29) is necessary rewritten into the form

$$Sh^*_{l_{\mathrm{D1}}} = \frac{\overline{k}_z \delta_{D,l_{\mathrm{D1}}}}{D} = K_\mathrm{L} \left(\frac{l_{\mathrm{D1}}}{l_{\mathrm{e1}}} \right) . \tag{56}$$

The only unknown quantity in the equation (55) is the normalized Sherwood number of the rear segment, whose behavior is influenced by forming a diffusion boundary layer over the front segment. Therefore, the Eq. (55) is possible to modify and define the normalized Sherwood number of the rear segment as

$$Sh^*_{2,l_{D2}} = \frac{\delta_{D,l_{D2}}}{1-a}\left(\frac{Sh^*_{l_D}}{\delta_{D,l_D}} - \frac{aSh^*_{1,l_{D1}}}{\delta_{D,l_{D1}}}\right). \tag{57}$$

The specific form of Eqs. (29), (56) and (57) for normalized Sherwood numbers depends on the choice of the characteristic lengths, l_D, l_{D1} and l_{D2}, of the individual segments and probe (the front, the rear, and the merged). However, for the arbitrary direction of simple shear flow, the characteristic length is no longer unambiguously geometrically determined as in the case of perpendicular flow. Now, its selection can be approached in several ways. In this work, we operate with two fundamental options of the l_D choice. The effective transfer length, l_e, is used in the first case, whereas the probe length, L_x, is applied in the second case (used already for the solution of perpendicular flow direction).

Solution based on the effective transfer length.

When the effective transfer length is used as a characteristic length, the thickness of the diffusion boundary layer at the front segment can be expressed as

$$\delta_{D,l_{\mathrm{e}1}} = \left(\frac{Dl_{\mathrm{e}1}}{\|\mathbf{S}\|}\right)^{\frac{1}{3}}, \tag{58}$$

and similarly for the rear segment and the merged probe as

$$\delta_{D,l_{D2}} = \delta_{D,l_\mathrm{e}} = \left(\frac{Dl_\mathrm{e}}{\|\mathbf{S}\|}\right)^{\frac{1}{3}}, \tag{59}$$

where l_e is the effective transfer length of the merged probe, $l_{\mathrm{e}1}$ is the effective transfer length of the front probe, and l_{D2} is the characteristic length of the rear probe. The thicknesses of diffusion boundary layers are thus assumed to be related to the distances from the starting positions of their formation.

The effective transfer length can be determined based on the relation (28), into which the proper lengths of individual electrodes are substituted. The

following expression can be obtained for the front probe

$$l_{\mathrm{e1}}^{\frac{1}{3}} = \begin{cases} \dfrac{L_{x1}^{\frac{1}{3}}}{(1-\beta)^{\frac{1}{6}}\left(1+\dfrac{aR\sqrt{\beta}}{5\sqrt{1-\beta}}\right)} & \text{for} \quad \beta \le \beta_{\mathrm{c1}} \\ \\ \dfrac{L_{x1}^{\frac{1}{3}}}{\beta^{\frac{1}{6}}a^{\frac{1}{3}}R^{\frac{1}{3}}\left(1+\dfrac{\sqrt{1-\beta}}{5aR\sqrt{\beta}}\right)} & \text{for} \quad \beta > \beta_{\mathrm{c1}} \end{cases} , \tag{60}$$

where β_{c1} denotes the critical value of the β parameter for the front probe, which is obtained by the same procedure as for the single probe, and its value can be expressed on the base of equation (4) as

$$\beta_{\mathrm{c1}} = \frac{1}{1+(aR)^2}\,. \tag{61}$$

The merged probe has an effective transfer length expressed in the form

$$l_{\mathrm{e}}^{\frac{1}{3}} = \begin{cases} \dfrac{L_{x}^{\frac{1}{3}}}{(1-\beta)^{\frac{1}{6}}\left(1+\dfrac{R\sqrt{\beta}}{5\sqrt{1-\beta}}\right)} & \text{for} \quad \beta \le \beta_{\mathrm{c}} \\ \\ \dfrac{L_{x}^{\frac{1}{3}}}{\beta^{\frac{1}{6}}R^{\frac{1}{3}}\left(1+\dfrac{\sqrt{1-\beta}}{5R\sqrt{\beta}}\right)} & \text{for} \quad \beta > \beta_{\mathrm{c}} \end{cases} . \tag{62}$$

By using effective transfer lengths, equation (57) can be rewritten in the form

$$Sh^*_{2,l_{\mathrm{e}}} = \frac{\delta_{D,l_{\mathrm{e}}}}{1-a}\left(\frac{Sh^*_{l_{\mathrm{e}}}}{\delta_{D,l_{\mathrm{e}}}} - \frac{aSh^*_{1,l_{\mathrm{e1}}}}{\delta_{D,l_{\mathrm{e1}}}}\right). \tag{63}$$

Substituting the relations (58) and (59) into the equation (63) then provides

$$Sh^*_{2,l_{\mathrm{e}}} = \frac{1}{1-a}\left[Sh^*_{l_{\mathrm{e}}} - aSh^*_{1,l_{\mathrm{e1}}}\left(\frac{l_{\mathrm{e}}}{l_{\mathrm{e1}}}\right)^{\frac{1}{3}}\right]. \tag{64}$$

The normalized Sherwood numbers on the right side of the equation (64) can be expressed in the simple form (see equations (29) and (56))

$$Sh^*_{l_{\mathrm{e}}} = Sh^*_{l_{\mathrm{e1}}} = K_{\mathrm{L}}\,. \tag{65}$$

Substituting Eq. (65) into Eq. (64) provides for the rear segment the dependence of normalized Sherwood number on the values of effective transfer lengths

$$Sh^*_{2,l_{\mathrm{e}}} = \frac{K_{\mathrm{L}}}{1-a}\left[1 - a\left(\frac{l_{\mathrm{e}}}{l_{\mathrm{e1}}}\right)^{\frac{1}{3}}\right]. \tag{66}$$

While $Sh^*_{l_e}$ and $Sh^*_{l_{e1}}$ values change neither with the probe geometry nor with the flow direction, Sh^*_{2,l_e} is a flow direction sensitive quantity through its dependence on the ratio of two effective transfer length, l_e/l_{e1} (see equations (60) and (62)). Moreover, each geometry of the two-strip probe is characterized by two critical dimensionless angles β_{c1} and β_c, see equations (61) and (4). Therefore, the final relation for Sh^*_{2,l_e}, which is obtained after substituting equations (60) and (62) into equation (66), is defined for three distinct regions of possible flow directions. These regions are delimited by β_{c1} and β_c values

$$Sh^*_{2,l_e} = \frac{\overline{k}_z \delta_{D,l_e}}{D} =$$

$$= \begin{cases} \dfrac{K_L}{1-a}\left[1 - \dfrac{a^{\frac{2}{3}}(5\sqrt{1-\beta} + aR\sqrt{\beta})}{5\sqrt{1-\beta} + R\sqrt{\beta}}\right] & \text{for} \quad \beta \le \beta_c \le \beta_{c1} \\ \dfrac{K_L}{1-a}\left[1 - \dfrac{\beta^{\frac{1}{3}} a^{\frac{2}{3}} R^{\frac{2}{3}}(5\sqrt{1-\beta} + aR\sqrt{\beta})}{(1-\beta)^{\frac{1}{3}}(\sqrt{1-\beta} + 5R\sqrt{\beta})}\right] & \text{for} \quad \beta_c < \beta \le \beta_{c1} \\ \dfrac{K_L}{1-a}\left[1 - \dfrac{\sqrt{1-\beta} + 5aR\sqrt{\beta}}{\sqrt{1-\beta} + 5R\sqrt{\beta}}\right] & \text{for} \quad \beta_c \le \beta_{c1} < \beta \end{cases} . \tag{67}$$

In the case of using effective transfer length for evaluating the normalized Sherwood number, the thickness of the diffusion boundary layer over the probe is correctly estimated. Therefore, the normalized Sherwood number value is accurately assessed from a physical point of view as the ratio of the convective mass transfer rate and diffusion mass transport rate. But the main disadvantage of this approach is that the average mass transfer coefficient is based on a combination of Eqs. (28), (59) and (67) is dependent on both $Sh^*_{l_e}(\beta)$ and $l_e(\beta)$. It follows that the behavior of the function $\overline{k}_z(\beta)$ is not proportional to $Sh^*_{l_e}(\beta)$ and thus the behavior of the average mass transfer coefficient cannot be deduced directly from the relation (67).

Solution based on the probe length.

Another option for choosing the characteristic lengths is to proceed in the same way as in the case of perpendicular flow direction. The thickness of the diffusion

boundary layer for the front segment is defined as

$$\delta_{D,L_{x1}} = \left(\frac{DL_{x1}}{\|\mathbf{S}\|} \right)^{\frac{1}{3}} . \tag{68}$$

The characteristic length for the rear segment is the same as that of the merged probe providing the boundary layer thickness

$$\delta_{D,L_x} = \left(\frac{DL_x}{\|\mathbf{S}\|} \right)^{\frac{1}{3}} . \tag{69}$$

Unlike the perpendicular flow, it is no longer possible to speak about the real thickness of the diffusion boundary layer because it is not formed only in the longitudinal direction, as is considered in Eqs. (68) and (69). In this case, some prolongation of the characteristic length due to a transverse flow component must be considered. Nevertheless, this complication in the perception of normalized Sherwood number has a practical justification. The main advantage of such a choice of characteristic length is the fact that its constant value is independent of the dimensionless angle β. Thus, the corresponding normalized Sherwood number is proportional to the mass transfer coefficient. The second reason for using this definition of characteristic length is that the probe size is applied for experimental data processing not only when the flow has a strictly perpendicular direction but also when the flow structure takes on a more complex form.

By introducing the relevant characteristic lengths into the investigated system, the equation (57) takes the form

$$Sh^*_{2,L_x} = \frac{\delta_{D,L_x}}{1-a} \left(\frac{Sh^*_{L_x}}{\delta_{D,L_x}} - \frac{aSh^*_{1,L_{x1}}}{\delta_{D,L_{x1}}} \right) . \tag{70}$$

Here again, the same thickness of the diffusion boundary layer is considered above the merged probe and its rear segment. After substitution equations (68) and (69) into equation (70), it is found the expression

$$Sh^*_{2,L_x} = \frac{Sh^*_{L_x} - a^{\frac{2}{3}} Sh^*_{1,L_{x1}}}{1-a} , \tag{71}$$

where the normalized Sherwood number for the merged probe and its front

segment can be expressed using equations (29) and (56) as

$$Sh^*_{L_x} = K_{\mathrm{L}} \left(\frac{L_x}{l_{\mathrm{e}}} \right)^{\frac{1}{3}}, \tag{72}$$

$$Sh^*_{L_{x1}} = K_{\mathrm{L}} \left(\frac{L_{x1}}{l_{\mathrm{e1}}} \right)^{\frac{1}{3}}. \tag{73}$$

After substitution equations (72) and (73) into equation (71), the defining relation for the normalized Sherwood number of the rear segment is obtained

$$Sh^*_{2,L_x} = \frac{K_{\mathrm{L}}}{1-a} \left[\left(\frac{L_x}{l_{\mathrm{e}}} \right)^{\frac{1}{3}} - a^{\frac{2}{3}} \left(\frac{L_{x1}}{l_{\mathrm{e1}}} \right)^{\frac{1}{3}} \right]. \tag{74}$$

where l_{e1} represents the effective transfer length of the front segment defined by the equation (60), and l_{e} represents the effective transfer length of the merged probe defined by the equation (62). By substituting the effective transfer lengths (equations (60) and (62)) into equation (74), the final expression for the dimensionless mass transfer coefficient of the rear segment is obtained

$$Sh^*_{2,L_x} = \frac{\overline{k}_z \delta_{D,L_x}}{D} =$$

$$= \begin{cases} \dfrac{K_{\mathrm{L}}(1-\beta)^{\frac{1}{6}}}{1-a} \left[1 - a^{\frac{2}{3}} + \dfrac{R\sqrt{\beta}}{5\sqrt{1-\beta}} \left(1 - a^{\frac{5}{3}} \right) \right] & \text{for} \quad \beta \le \beta_{\mathrm{c}} \le \beta_{\mathrm{c1}} \\ \dfrac{K_{\mathrm{L}}}{1-a} \left[\beta^{\frac{1}{6}} R^{\frac{1}{3}} \left(1 + \dfrac{\sqrt{1-\beta}}{5R\sqrt{\beta}} \right) - a^{\frac{2}{3}} (1-\beta)^{\frac{1}{6}} \left(1 + \dfrac{aR\sqrt{\beta}}{5\sqrt{1-\beta}} \right) \right] & \text{for} \quad \beta_{\mathrm{c}} < \beta \le \beta_{\mathrm{c1}} \\ K_{\mathrm{L}} \beta^{\frac{1}{6}} R^{\frac{1}{3}} & \text{for} \quad \beta_{\mathrm{c}} \le \beta_{\mathrm{c1}} < \beta \end{cases}. \tag{75}$$

The main advantage of choosing L_x as a characteristic length is that the dependence between $\overline{k}_z$ and Sh^*_{2,L_x} is directly proportional for any specific geometry of the two-strip probe.

Mass transfer on the individual segments of the probe.

Two different approaches to Sherwood number normalization, given by Eqs. (67) and (75), are compared in Figures 5 and 6, where it is demonstrated how both these nondimensional numbers, $Sh_{2,l_{\mathrm{e}}}$ and Sh_{2,L_x}, vary with the change of

probe geometry (R, a) and flow direction (β). Also seen in these figures are the dependencies of critical dimensionless angles β_{c} and β_{c1}, see solid and dashed curves, respectively, on the probe aspect ratio R. As the length of the front segment is enlarged ($L_{x1} \to L_x$), both these curves are gradually merging.

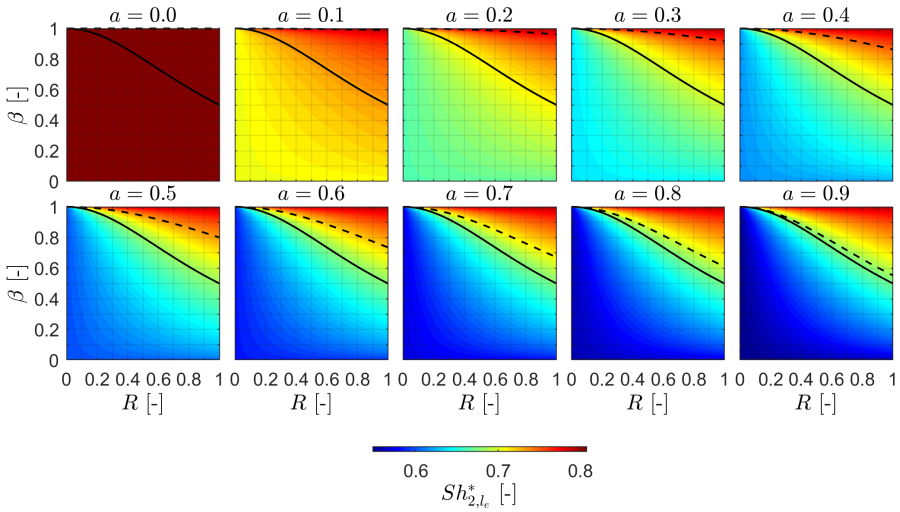

Figure 5: Normalized Sherwood number of the front ($a = 0$) and the rear ($a = 0.1-0.9$) probes with characteristic length l_{e} as a function of dimensionless angle β and geometrical aspect ratio R for different values of dividing coefficient a, see Eq. (67). The black curve represents values of the critical dimensionless angle of the merged electrode β_{c}, and the dashed black curve represents values of the critical dimensionless angle of the front electrode β_{c1}.

Figure 5 shows the normalized Sherwood number, $Sh_{2,l_{\mathrm{e}}}$ based on the characteristic length l_{e}. As for $a = 0$, the system consists of only a single probe; the following relation holds

$$Sh^*_{1,l_{\mathrm{e}1}} = Sh^*_{2,l_{\mathrm{e}}}(a = 0, \forall R, \forall \beta) = K_{\mathrm{L}}\,, \tag{76}$$

and the normalized Sherwood number is constant for any probe geometry and flow direction, see the upper-left sub-figure. When the dividing coefficient a is increased, the length of front segment L_{x1} is increased at the expense of rear one, L_{x2}, and the value of $Sh_{2,l_{\mathrm{e}}}$ decreases. On the other hand, the value of $Sh_{2,l_{\mathrm{e}}}$ increases when the flow direction changes from longitudinal to transverse

one (and β increases). Therefore, the minimum values of Sh_{2,l_e} are found under conditions when $\beta = 0$ (longitudinal flow) and $R \to 0$ (thin strip probe), whereas the maximum values are found for $\beta = 1$ (transverse flow) and $R \to 1$ (square probe). In the case of transverse flow, $\beta = 1$, the concentration wake arising over the front strip does not affect the concentration field at the rear strip and thus the value of Sh^*_{2,l_e} is independent of the dividing coefficient a.

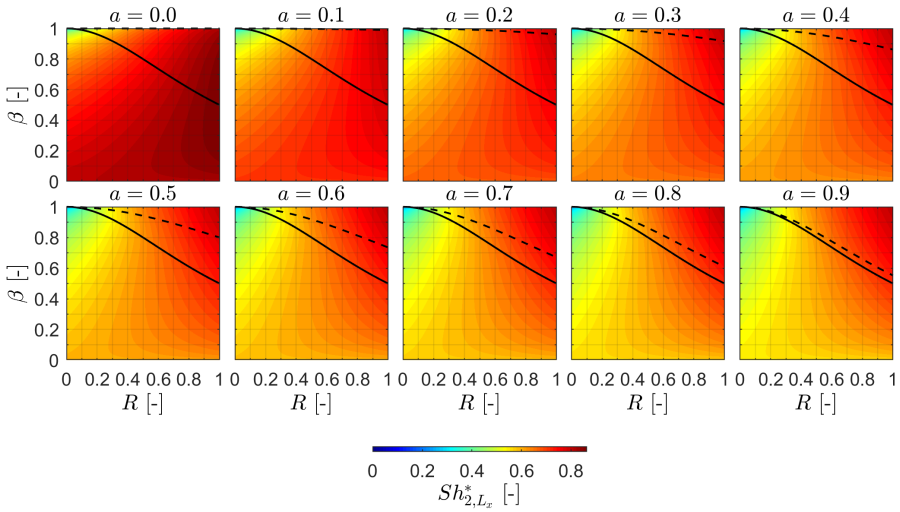

Figure 6: Normalized Sherwood number of the front ($a = 0$) and the rear ($a = 0.1-0.9$) probes with characteristic length L_x as a function of dimensionless angle β and geometrical aspect ratio R for different values of dividing coefficient a, see Eq. (75). The black curve represents values of the critical dimensionless angle of the merged electrode β_c, and the dashed black curve represents values of the critical dimensionless angle of the front electrode β_{c1}.

Figure 6 presents the normalized Sherwood number Sh_{2,L_x} based on the characteristic length L_x. The distributions of Sherwood number values are different from that presented in Figure 5. In the case of a single probe ($a = 0$), the normalized Sherwood number is not constant, see the upper-left sub-figure, but its value depends on the ratio of two characteristic lengths according to the relation

$$Sh^*_{1,L_x} = Sh^*_{2,L_x}(a = 0, \forall R, \forall \beta) = K_L \left(\frac{L_x}{l_e} \right)^{\frac{1}{3}}, \tag{77}$$

where the effective transfer length l_e defined by Eq. (62) changes with actual

values of R and β. The normalized Sherwood number Sh^*_{2,L_x} again decreases with increasing the dividing coefficient a. The minimum mass transport rates are found for $\beta = 1$ (transverse flow) and $R \to 0$ (thin strip probe), whereas the maximum mass transport rates are achieved for $R \to 1$ (square probe). The value of dimensionless angle β needed to reach this maximum mass transport depends on the actual value of dividing coefficient a.

As seen from the inspection of Eqs. (69) and (75), the average mass transfer coefficient is proportional to the normalized Sherwood number based on the probe length according to the relation

$$\overline{k}_z = KSh^*_{L_x}\,, \tag{78}$$

where for given flow conditions, the parameter K is a constant calculated according to the simple formula

$$K = \frac{D^{\frac{2}{3}}\|\mathbf{S}\|^{\frac{1}{3}}}{L_x^{\frac{1}{3}}}\,. \tag{79}$$

This proportionality has fundamental importance when Sh^*_{2,L_x} is used for the direct interpretation of mass transport rates on the two-strip probe. Generally, the most significant mass transport occurs near the leading edges of the probe and it is enhanced by convection, which makes the diffusion boundary layer thinner. The convection is represented by the wall shear rate vector, whose components (longitudinal and transverse) control the diffusion boundary layer development at the probe edges. Therefore, to interpret the mass transport rate qualitatively, the average mass transfer coefficient can be expressed as a sum of two components

$$\overline{k}_z \sim \frac{1}{L_x L_y}\left(\int_0^{L_x} \mathbf{S}\cdot\mathbf{n}_y \mathrm{d}l + \int_0^{L_y} \mathbf{S}\cdot\mathbf{n}_x \mathrm{d}l\right)\,, \tag{80}$$

where $\mathbf{n}_x \equiv (1,0,0)$ and $\mathbf{n}_y \equiv (0,1,0)$ are unit vectors normal to the probe sides. Expressing the dot product provides the relation

$$\overline{k}_z \sim \frac{\int_0^{L_x} S_y \mathrm{d}l + \int_0^{L_y} S_x \mathrm{d}l}{L_x L_y} = \frac{S_y}{L_y} + \frac{S_x}{L_x} = \frac{\frac{\sqrt{\beta}}{L_y} + \frac{\sqrt{1-\beta}}{L_x}}{\sqrt{S_x^2 + S_y^2}}\,, \tag{81}$$

where wall shear rate vector components are evaluated using Eq. (3). This expression implies how the mass transport depends on the mutual orientation between the probe and flow direction. This interpretation of mass transport is suitable for front segments or merged probes ($a = 0$). To keep proportionality relationship between mass transfer coefficient and normalized Sherwood number, the longitudinal dimension L_x needs to be fixed value, to preserve constant characteristic dimension. Therefore on studied interval of aspect ratios it is possible to change only values of transverse dimension L_y. In correspondence with R-axis, the transverse dimension lies in interval $L_y \in \langle L_x, \infty)$ and in accordance to equation (81) maximal $\overline{k}_z$ is found for minimal possible L_y that is $L_y = L_x$ or in other words $R = 1$. From this consideration for front or merged probes the maximal mass transfer for an arbitrary flow direction occurs for the maximal possible aspect ratio, which corresponds with Fig. 6 for $a = 0$.

To receive a global maximum, the equation (81) is for fixed L_x, $R = 1$ and for a given magnitude of velocity field u possible to rewrite to

$$\overline{k}_z \sim \text{const}(\sqrt{\beta} + \sqrt{1-\beta})\,, \tag{82}$$

and for $\forall\beta$ extreme is received by derivative with respect to the dimensionless angle β and looking for a root. After adjustments is received

$$\frac{\partial \overline{k}_z}{\partial \beta} = \frac{1}{\sqrt{\beta}} - \frac{1}{\sqrt{1-\beta}} = 0\,, \tag{83}$$

which holds true for $\beta = 0.5$. In the discovered system ($a = 0, R = 1, \beta = 0.5$) the most intense contact between edges of the electrode and onflowing liquid is achieved and as a consequence mass transfer rate is maximalizied see Fig. 6 for $a = 0$.

The question is to what extent the convection through the transverse leading edge L_y should be involved in the mass transport taking place on the rear segment. As the dividing coefficient a increases, a significant decrease of mass transfer rates is observed when the flow with dominant longitudinal velocity component u_x is applied, see Fig. 6 for $a > 0$. It is a consequence of a significant

concentration wake produced due to the mass transfer at the front segment. In general, for small a values, the effect of longitudinal convection on the mass transport on the rear probe is still considerable, but its significance decreases remarkably with increasing the dividing coefficient. Thus, as the a coefficient increases, the importance of the second term ($\sqrt{1-\beta}/L_x$) in the equation (81) decreases. The equation (81) can be, therefore, generalized into the form

$$\overline{k}_z \sim \frac{\dfrac{\sqrt{\beta}}{L_y} + f(a)\dfrac{\sqrt{1-\beta}}{L_x}}{\sqrt{S_x^2 + S_y^2}}\,, \tag{84}$$

where $f(a)$ is a decreasing function of the division coefficient a. Its value ranges from 0 (for $a \to 1$) to 1 (for $a = 0$).

2.3.3. Numerical validation of the analytical solution

To confirm the correctness of the derived theory described by equations (67) and (75) for normalized Sherwood numbers of the two-segmented probe, the numerical solution of the studied problem is done. The mass transport in the viscous boundary layer built due to the simple shear flow at the wall with a two-strip probe is modeled. The concentration field necessary to evaluate the normalized Sherwood number was obtained numerically by solving the equation (11), which is modified into a dimensionless form (see our previous work [1])

$$z^+\frac{\partial c^+}{\partial x^+} + z^+\frac{\sqrt{\beta}R}{\sqrt{1-\beta}}\frac{\partial c^+}{\partial y^+} = \frac{L_x}{l_D\sqrt{1-\beta}}\frac{\partial^2 c^+}{(\partial z^+)^2}\,, \tag{85}$$

where

$$x^+ = \frac{x}{L_x}\,, \quad y^+ = \frac{y}{L_y}\,, \quad z^+ = \frac{z}{\delta_{D,l_D}}\,, \quad c^+ = \frac{c - c_\mathrm{w}}{c_\infty - c_\mathrm{w}}\,. \tag{86}$$

Velocity components in the convection terms on the left side of the equation (85) are substituted by Eq. (8). The simulated domain has a cuboidal shape. The bottom of this domain is represented by the wall with the two-segmented probe. Its height is chosen to be sufficient not to restrict the formation of a diffusion boundary layer above the probe. Boundary conditions taken into account for non-dimensional concentration are: (i) on the surface of probes is $c^+ = 0$; (ii)

in the inlet is $c^+ = 1$; (iii) outlet is defined as $\nabla^+ c^+ = 0$; (iv) in the top wall is $c^+ = 1$, and (v) the bottom wall except for the surface of the two-segmented probe is equal to $\partial c^+ / \partial z^+ = 0$.

For discretization, the finite volume method is employed by hexahedral computational cells. In addition, a nonuniform computational grid is used, which enabled the grid refinement in zones of the leading edges of the electrode because the most significant gradients of dimensionless concentration c^+ are occurred in these locations. The number of the computational grid cells moves from 2.10^6 to 2.10^7 depending on the dividing coefficient a. The UPWIND scheme for convection terms and the central differencing scheme for the diffusion term are used for discretization. The solution of a system of linear algebraic equations is performed by smoothSolver with the preconditioner method DILU (Simplefied diagonal-based incomplete LU smoother for asymmetric matrices). Numerical simulations are done by the OpenFOAM software in which the solver for Eq.(85) solution was programmed.

The studied parametric space (R, β, a) is sampled in the following way: $R \in \langle 0.1, 1 \rangle$ with $\Delta R = 0.1$; $\beta \in \langle 0, 1 \rangle$ with $\Delta \beta = 0.1$, and $a \in \langle 0.1, 0.9 \rangle$ with $\Delta a = 0.1$. To cover the whole parametric space, in complete 990 simulations were performed. Their results were compared with the analytical predictions based on mass transfer coefficient values. In the case of the numerical solution, the mass transfer coefficients are obtained from the concentration fields by the following integrations

$$\overline{k}_{z1} = \frac{D}{aL_x L_y} \int_0^{aL_x} \int_0^{L_y} \left(\frac{\partial c^+}{\partial z} \right) \mathrm{d}y \, \mathrm{d}x \,, \tag{87}$$

$$\overline{k}_{z2} = \frac{D}{(1-a)L_x L_y} \int_{aL_x}^{L_x} \int_0^{L_y} \left(\frac{\partial c^+}{\partial z} \right) \mathrm{d}y \, \mathrm{d}x \,. \tag{88}$$

Analytical values of mass transfer coefficients are obtained by adjusting the equations (51) and (52) into the forms

$$\overline{k}_{z1} = \frac{DSh^*_{1,l_{D1}}}{\delta_{D,l_{D1}}} = \frac{DSh^*_{1,L_{x1}}}{\delta_{D,L_{x1}}} = \frac{DSh^*_{1,l_{\mathrm{e}1}}}{\delta_{D,l_{\mathrm{e}1}}} \,, \tag{89}$$

$$\overline{k}_{z2} = \frac{DSh^*_{2,l_{D2}}}{\delta_{D,l_{D2}}} = \frac{DSh^*_{2,L_x}}{\delta_{D,L_x}} = \frac{DSh^*_{2,l_{\mathrm{e}}}}{\delta_{D,l_{\mathrm{e}}}} \,. \tag{90}$$

As it follows from the equations (89) and (90), values of mass transfer coefficients calculated from the analytical formulas are not dependent on the choice of characteristic lengths used to determine the thickness of diffusion boundary layers. The difference between $\overline{k}_z$ results obtained from the analytical and numerical solutions varied from 10^{-4} to 10^{-5} (thus being smaller than ?? percents). A further reduction of the error could be achieved by using a denser numerical grid, especially in the area of the leading edges of the probe. The agreement between the numerical and analytical results proves the validity of Eqs. (67) and (75) for the description of convective mass transport at the two-strip probe for any aspect ratio R, dividing coefficient a, and flow direction β.

3. Application of two-strip probes for directionally sensitive measurements

The measurement with a two-strip probe provides two electric current signals, which are collected from two strip segments. The question is how these signals can be converted into information about actual near-wall flow, i.e., how to determine the magnitude, $\|\mathbf{S}\|$, and direction, β, of wall shear rate. However, before introducing the procedure of possible data treatment, a small reflection on the symmetry of derived analytical solutions and its consequence for flow direction measurements is presented.

As already discussed above (see section 2.2), a single strip probe exhibits two types of symmetry concerning the flow. Their axes are identical to the probe axes (thus, x-axis for left/right flow and y-axis for frontal/reversal flow symmetry). For this reason, the strip probe can only measure the flow angle $\alpha \in \langle 0, \pi/2 \rangle$, thus the flow direction in the range of $\beta \in \langle 0, 1 \rangle$.

Using the two-strip probe (see Fig. 7), the x-axis symmetry is preserved and the probe is still unable to distinguish between flows with α and $-\alpha$ angles because the equality $\overline{k}_z(\alpha) = \overline{k}_z(-\alpha)$ holds. On the other hand, the y-axis symmetry disappears because the ratio $\overline{k}_{z2}/\overline{k}_{z1}$ can be used to distinguish between frontal and reversal flows. In general, if $\overline{k}_{z2}/\overline{k}_{z1} < 1$, the front segment

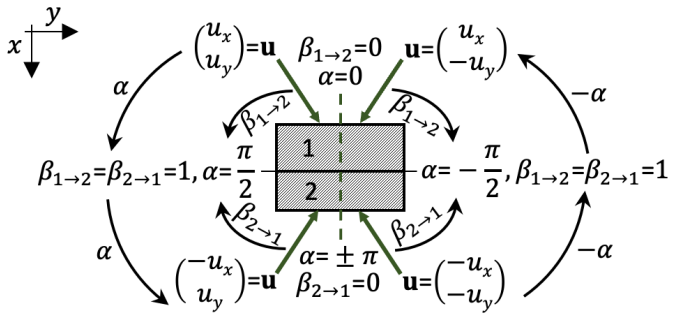

Figure 7: Scheme of two-strip probe: (i) the measuring symmetry of the fluid flow angle where the axis of symmetry is the green dashed line; (ii) the relation between the dimensionless angle β and the angle α; $\beta_{1\to2}$ describes the frontal flow for $\alpha \in \langle 0, \pi/2\rangle$ and $\beta_{2\to1}$ describes the reversal flow for $\alpha \in \langle \pi/2, \pi\rangle$.

is considered as an independent probe, which influences the concentration field at the rear segment. If $\overline{k}_{z2}/\overline{k}_{z1} > 1$, the behavior of both segments is switched. The rear segment starts to be independent, and the front segment is affected by the concentration wake from the rear segment. If $\overline{k}_{z2}/\overline{k}_{z1} = 1$, the purely transverse flow is observed ($\beta = 1$), and both probes behave independently and do not affect each other. Thus, the flow direction on the interval $\alpha \in \langle 0, \pi\rangle$ can be measured with the two-strip probe.

To further extend the interval of flow angle measurements, a multi-segment probe or a two-strip probe with an artificially created asymmetry in the y-direction must be used, for example, by shifting the rear segment relative to the front one. Both these topics will be addressed in our future works. If during the measurement of the wall shear rate vector, it can be assumed that the mean flow direction is clearly defined, by turning the two-strip probe by $\pi/2$, a measuring system of electrodes can be obtained that it can evaluate the angle of the fluid flow in the range of $\alpha \in \langle -\pi/2, \pi/2\rangle$. In this way, the main handicap of the two-strip probe can be suppressed.

The definition of the dimensionless angle β based on equation (3) implies that this variable cannot take values greater than 1. Therefore, if necessary for clarity in the text to distinguish between the flow situations for $\overline{k}_{z2}/\overline{k}_{z1} \leq 1$

(frontal flow) and for $\overline{k}_{z2}/\overline{k}_{z1} > 1$ (reversal flow), the symbol $\beta_{1\to2}$ and $\beta_{2\to1}$ are used instead of β, see Fig. 7.

3.1. Determination of wall shear rate vector

Based on the combination of relations (89) and (90) with Eq. (30), it is possible to obtain for both strip segments corresponding equations relating the measured average mass transfer coefficient with the wall shear rate vector

$$\frac{\overline{k}_{z1}}{D^{\frac{2}{3}}\|\mathbf{S}\|^{\frac{1}{3}}} = \frac{Sh^*_{1,l_{D1}}}{l^{\frac{1}{3}}_{D1}} = \frac{Sh^*_{1,L_{x1}}}{L^{\frac{1}{3}}_{x1}} = \frac{Sh^*_{1,l_{\mathrm{e}1}}}{l^{\frac{1}{3}}_{\mathrm{e}1}}\,, \tag{91}$$

$$\frac{\overline{k}_{z2}}{D^{\frac{2}{3}}\|\mathbf{S}\|^{\frac{1}{3}}} = \frac{Sh^*_{2,l_{D2}}}{l^{\frac{1}{3}}_{D2}} = \frac{Sh^*_{2,L_x}}{L^{\frac{1}{3}}_{x}} = \frac{Sh^*_{2,l_{\mathrm{e}}}}{l^{\frac{1}{3}}_{\mathrm{e}}}\,. \tag{92}$$

As it turns out from the equations 91 and 92, the average mass transfer coefficient is independent of the choice of characteristic length l_{D1} and l_{D2}, but it is dependent on both the wall shear rate magnitude, $\|\mathbf{S}\|$, and the flow direction, β. To obtain one equation with only one independent variable β, equation (92) is divided by equation(91)

$$\frac{\overline{k}_{z2}}{\overline{k}_{z1}} = \frac{Sh^*_{2,l_{D2}} l^{\frac{1}{3}}_{D1}}{Sh^*_{1,l_{D1}} l^{\frac{1}{3}}_{D2}}\,. \tag{93}$$

To determine the flow direction on the whole interval $\alpha \in \langle 0, \pi\rangle$, it is necessary to use two sets of analytical formulas, which consider the order of individual strip segments relative to the flow direction. In the first case, equations cover the interval $\alpha \in \langle 0, \pi/2\rangle$. For this mean flow direction, the frontal designation flow is used, and fluid flows over the front electrode in the direction to the rear one. The second case deals with the interval $\alpha \in \langle \pi/2, \pi\rangle$, and it is identified as the reversal flow. Fluid flows at first over the rear electrode and then to the front one. The transverse flow ($\alpha = \pi/2$) represents a limiting case when the frontal flow changes to the reversal flow and vice versa.

3.1.1. Frontal flow

When normalized Sherwood numbers are introduced into the equation (93) (applying either equations (65) and (66) or equations (73) and (74)), the fol-

lowing relation can be obtained

$$\frac{\overline{k}_{z2}}{\overline{k}_{z1}} = \frac{1}{1-a}\left[\left(\frac{l_{\mathrm{e1}}}{l_{\mathrm{e}}}\right)^{\frac{1}{3}} - a\right] = g(\beta)\,, \tag{94}$$

where $g(\beta)$ stands for an auxiliary function, which is for each probe geometry dependent only on one parameter β. After substituting effective transfer lengths l_{e} and l_{e1} from Eqs. (62) and (60) into Eq. (94), three specific forms of Eq. (94) are obtained

$$g(\beta) = \begin{cases} \dfrac{1}{1-a}\left[\dfrac{a^{\frac{1}{3}}(5\sqrt{1-\beta}+R\sqrt{\beta})}{5\sqrt{1-\beta}+aR\sqrt{\beta}} - a\right] & \text{for} \quad \beta \le \beta_{\mathrm{c}} \le \beta_{\mathrm{c1}} \\ \dfrac{1}{1-a}\left[\dfrac{a^{\frac{1}{3}}(1-\beta)^{\frac{1}{3}}(\sqrt{1-\beta}+5R\sqrt{\beta})}{R^{\frac{2}{3}}\beta^{\frac{1}{3}}(5\sqrt{1-\beta}+aR\sqrt{\beta})} - a\right] & \text{for} \quad \beta_{\mathrm{c}} < \beta \le \beta_{\mathrm{c1}} \\ \dfrac{1}{1-a}\left[\dfrac{a(5R\sqrt{\beta}+\sqrt{1-\beta})}{5aR\sqrt{\beta}+\sqrt{1-\beta}} - a\right] & \text{for} \quad \beta_{\mathrm{c}} \le \beta_{\mathrm{c1}} < \beta \end{cases} . \tag{95}$$

Based on the expressions mentioned above, Fig. 8, shows the dependence of ratio $\overline{k}_{z2}/\overline{k}_{z1}$ as a function of parameter β, aspect ratio R and dividing coefficient a. The value of ratio $\overline{k}_{z2}/\overline{k}_{z1}$ is found to be augmented with increasing both, the dividing coefficient a and aspect ratio R. In both cases, it is caused by the fact that an increase in the strip length is accompanied by an decrease in the averaged mass transfer coefficient and this reduction is more important for the front strip (because rapid development of the boundary layer takes place there). Minimal values of ratio $\overline{k}_{z2}/\overline{k}_{z1}$ are observed for the perpendicular flow ($\beta = 0$) because, in this case, the concentration wake of the front strip has the most significant impact on the mass transfer on the rear strip. On the other hand, maximal values of $\overline{k}_{z2}/\overline{k}_{z1}$ can be found for the transverse flow ($\beta = 1$) when both the strips are not affecting each other and the ratio $\overline{k}_{z2}/\overline{k}_{z1}$ is always equal to 1.

3.1.2. Reversal flow

For the reversal flow, the initial expression for a description of ratio $\overline{k}_{z2}/\overline{k}_{z1}$ is again Eq. (93). However, because the flow direction is now opposite to the case

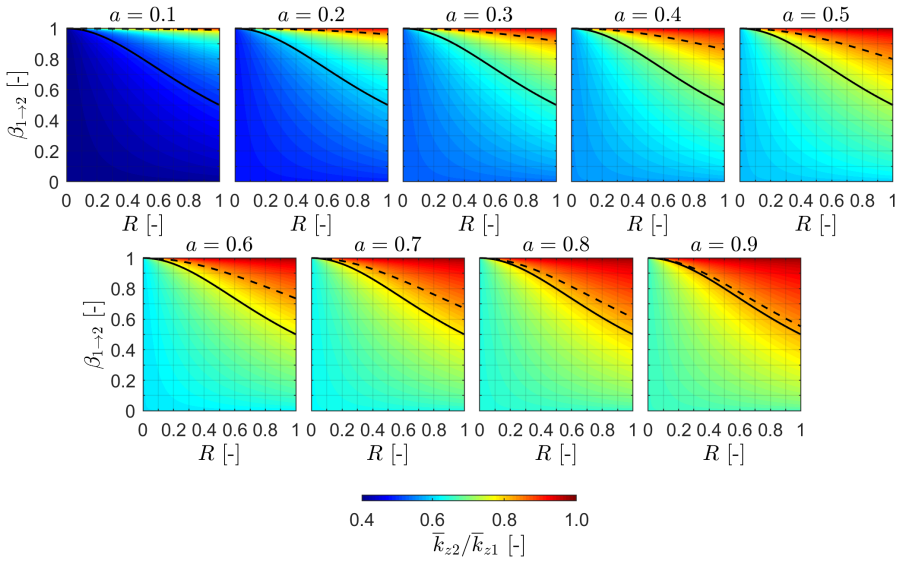

Figure 8: Ratio of mass transfer coefficients of rear and front electrode as a function of frontal dimensionless angle $\beta_{1\to2}$ and geometrical aspect ratio R for different values of dividing coefficient a. The black curve represents values of the critical dimensionless angle of the merged electrode β_{c}, while the dashed black curve represents values of the critical dimensionless angle of the front electrode β_{c1}.

of frontal flow, the order of individual segments has to be changed appropriately. Therefore, the rear strip needs to be treated as the front one and, analogously, the front strip as the rear one. For this reason, the original relations describing the ratio of mass transfer coefficients $\overline{k}_{z2}/\overline{k}_{z1}$ must be modified in such a way, that their analytical formulations correspond with the current switched order of segments. With usage of auxiliary index notation for dimensionless angles, this conversion leads to the equality

$$\left(\frac{\overline{k}_{z2}}{\overline{k}_{z1}}\right)_{\beta_{2\to1}} = \left(\frac{\overline{k}_{z1}}{\overline{k}_{z2}}\right)_{\beta_{1\to2}} . \tag{96}$$

Further, it is necessary to take into consideration the impact of reversed order of segments also on the value of dividing coefficient a. Therefore, its formulation on the right side of equation (96) is now represented by expression $1-a$, instead of the original value a used on its left side. By considering the above mentioned

assumptions in equation (95), its alternative for the case of reversal flow is obtained in the form of following relationships

$$g(\beta) = \begin{cases} a\left[\dfrac{(1-a)^{\frac{1}{3}}(5\sqrt{1-\beta}+R\sqrt{\beta})}{5\sqrt{1-\beta}+(1-a)R\sqrt{\beta}} - 1 + a\right]^{-1} & \text{for} \quad \beta \leq \beta_{\mathrm{c}} \leq \beta_{\mathrm{c2}} \\ a\left[\dfrac{(1-a)^{\frac{1}{3}}(1-\beta)^{\frac{1}{3}}(\sqrt{1-\beta}+5R\sqrt{\beta})}{R^{\frac{2}{3}}\beta^{\frac{1}{3}}(5\sqrt{1-\beta}+(1-a)R\sqrt{\beta})} - 1 + a\right]^{-1} & \text{for} \quad \beta_{\mathrm{c}} < \beta \leq \beta_{\mathrm{c2}} \\ a\left[\dfrac{(1-a)(5R\sqrt{\beta}+\sqrt{1-\beta})}{5(1-a)R\sqrt{\beta}+\sqrt{1-\beta}} - 1 + a\right]^{-1} & \text{for} \quad \beta_{\mathrm{c}} \leq \beta_{\mathrm{c2}} < \beta \end{cases}, \tag{97}$$

where β_{c2} is the critical value of the β parameter for the rear strip at reversal

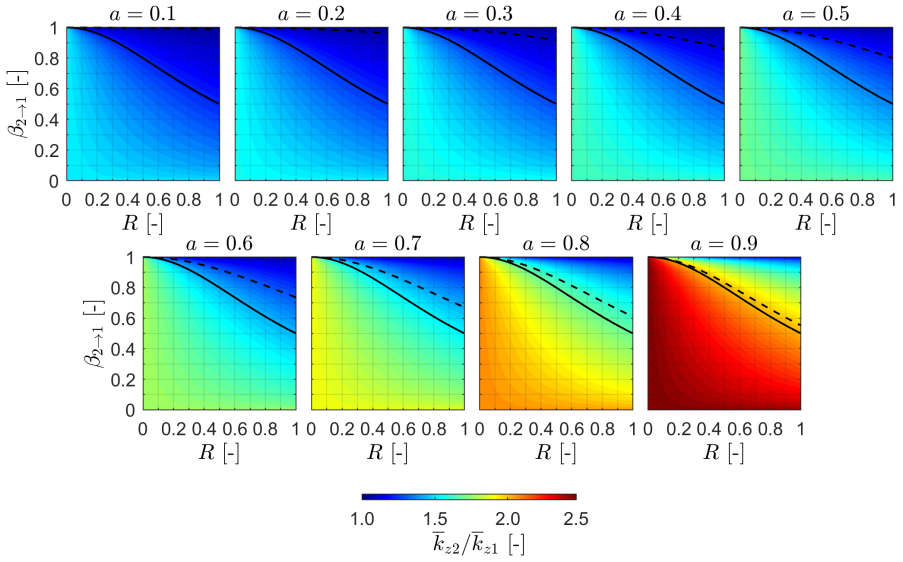

Figure 9: Ratio of mass transfer coefficients of rear and front electrode as a function of reversal dimensionless angle $\beta_{2\to1}$ and geometrical aspect ratio R for different values of dividing coefficient a. The black curve represents values of the critical dimensionless angle of the merged electrode β_{c}, while the dashed black curve represents values of the critical dimensionless angle of the rear electrode β_{c2}.

flow conditions. It is defined by analogy to Eq. (61) as

$$\beta_{c2} = \frac{1}{1 + [(1-a)R]^2} \,. \tag{98}$$

Ratios of average mass transfer coefficients $\overline{k}_{z2}/\overline{k}_{z1}$ as a function of parameter β, aspect ratio R and dividing coefficient a are shown in Fig. 9. As the roles of both segments are switched in comparison to the frontal flow arrangement, the ratio of average mass transfer coefficients for the reversal flow reaches larger values, compare Figs. 8 and 9. It always applies that $\overline{k}_{z2}/\overline{k}_{z1} \geq 1$. The value of ratio $\overline{k}_{z2}/\overline{k}_{z1}$ is again augmented with increasing the dividing coefficient a. However, all other trends observed in Fig. 9 are opposite to those in Fig. 8. The maximal values of $\overline{k}_{z2}/\overline{k}_{z1}$ are found for the case of perpendicular flow ($\beta = 0$), minimal values of ratio $\overline{k}_{z2}/\overline{k}_{z1}$ are connected with the transverse flow ($\beta = 1$), and the higher aspect ratio R brings about the lower value of ratio $\overline{k}_{z2}/\overline{k}_{z1}$.

3.1.3. Determination of wall shear rate from measured electric currents

The average mass transfer coefficients $\overline{k}_{z1}$ and $\overline{k}_{z2}$ are obtained from the measured electric currents. Faraday's law (1) in combination with Eq. (2) is applied for this purpose. For a specific probe geometry, the only unknown quantity in the functions defined either by equation (95) (for $\overline{k}_{z2}/\overline{k}_{z1} \leq 1$) or (97) (for $\overline{k}_{z2}/\overline{k}_{z1} > 1$) is the parameter β. To solve the problem, the root of function $g(\beta) - \overline{k}_{z2}/\overline{k}_{z1}$ has to be find. On the studied interval $\beta \in \langle 0, 1 \rangle$, this nonlinear function has only one real β root, which can be found by any iterative numerical method, such as Newton's method.

With the known value of parameter β, equation (3) is used to calculate the angle α corresponding to actual flow direction. It provides for the case of frontal flow

$$\alpha = \arccos(\sqrt{\beta_{1\to2}}) \,, \tag{99}$$

whereas for the case of reversal flow

$$\alpha = \pi - \arccos(\sqrt{\beta_{2\to1}}) \,. \tag{100}$$

When the dimensionless angle β is known, the equations (91) is applied to calculate the magnitude of wall shear rate, $\|\mathbf{S}\|$. Wall shear stress τ_{w} can be directly received by multiplying $\|\mathbf{S}\|$ by the value of dynamic viscosity μ of given liquid.

3.2. Optimal configuration of the two-strip probe

In the previous text, the theory necessary to evaluate the experimental measurements was presented, as well as the relations, based on which the measured currents can be used to obtain the shear rate vector. In this section, the current ratios predicted for various probe geometries will be analyzed with the aim to find out an optimal probe configuration with respect to the sensitivity of flow direction measurement.

Figure 10 shows how the ratio between electric currents from the second (I_2) and first (I_1) strip depends on the geometric parameters R and a. This figure covers the whole interval of flow angles $\alpha \in \langle 0, \pi \rangle$, which is divided into two parts: $\beta_{1\to 2} \in \langle 0, 1 \rangle$ or $\alpha \in \langle 0, \pi/2 \rangle$ (for frontal flow), and $\beta_{2\to 1} \in \langle 1, 0 \rangle$ or $\alpha \in \langle \pi/2, \pi \rangle$ (for reversal flow), see eqs. (34) and (100) or Fig. 7. The dividing coefficient a affects strongly the range of $I_2/I_1(\beta)$ values seen in Fig. 10. This parameter also determines the critical value of I_2/I_1 reached when the flow changes its direction from frontal to reversal one ($\beta = \beta_{1\to 2} = \beta_{2\to 1} = 1$). This critical value can be calculated according to the following relation

$$\left(\frac{I_2}{I_1}\right)_{\mathrm{crit}} = \frac{1-a}{a}\,, \tag{101}$$

where the fraction $\frac{1-a}{a}$ represents the ratio between second and first strip surface areas (thus the multiplier used also to convert $\overline{k}_{z2}/\overline{k}_{z1}$ into I_2/I_1 ratio). The critical values corresponding to the values of $a = 0.1$, 0.5, and 1 are in the figure delimited by horizontal blue lines. Obviously, with increasing dividing coefficient a, the value of critical current ratio gradually decreases to zero.

While with the change of parameter a the course of $I_2/I_1(\beta)$ dependence is just slightly modified, the influence of parameter R is much stronger. Concerning R, two limiting cases can be distinguished, namely $R \to 0$ and $R \to \infty$. In

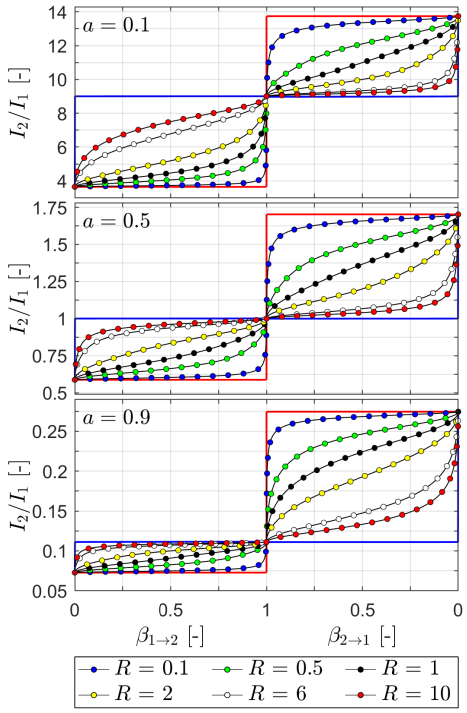

Figure 10: The ratio of electric currents flowing through the rear and front segments as functions of the dimensionless angles $\beta_{1\to2}$ and $\beta_{1\to2}$ for different values of aspect ratio R and dividing coefficient a. The red lines represent limit case $R \to 0$; the Blue lines symbolizes limit case $R \to \infty$.

both these cases, the two-strip probe is practically insensitive to the change in flow direction. In the first case ($R \to 0$, see red lines in Fig. 10), its only change is a sharp increase from $I_2/I_{1_{min}}$ to $I_2/I_{1_{max}}$ at $\beta = 1$ (transverse flow). In the second case ($R \to \infty$, see blue lines in Fig. 10), an oscillation between values $I_2/I_{1_{min}}$ and $I_2/I_{1_{max}}$ is observed at $\beta = 0$ (frontal or reversal flow). These minimum $I_2/I_{1_{min}}$ and maximum $I_2/I_{1_{max}}$ values are dependent only on the parameter a and for frontal flow region (see also equation (45)) it holds

$$\left(\frac{I_2}{I_1}\right)_{\min} = a^{-\frac{2}{3}} - 1 \tag{102}$$

and analogically for reversal flow region

$$\left(\frac{I_2}{I_1}\right)_{\max} = \frac{1}{(1-a)^{-\frac{2}{3}} - 1}. \tag{103}$$

The extreme values of current ratio are for different values of a listed in Tab. 1.

a	$\left(\frac{I_2}{I_1}\right)_{\min}$	$\left(\frac{I_2}{I_1}\right)_{\text{crit}}$	$\left(\frac{I_2}{I_1}\right)_{\max}$	$\frac{(I_2/I_1)_{\text{crit}}}{(I_2/I_1)_{\min}}$	$\frac{(I_2/I_1)_{\max}}{(I_2/I_1)_{\text{crit}}}$	$\frac{(I_2/I_1)_{\max}}{(I_2/I_1)_{\min}}$
0.1	3.64	9.00	13.74	2.47	1.53	3.77
0.2	1.92	4.00	6.23	2.08	1.56	3.24
0.3	1.23	2.33	3.73	1.89	1.60	3.03
0.4	0.84	1.50	2.46	1.78	1.64	2.93
0.5	0.59	1.00	1.70	1.70	1.70	2.90
0.6	0.41	0.67	1.19	1.64	1.78	2.93
0.7	0.27	0.43	0.81	1.60	1.89	3.03
0.8	0.16	0.25	0.52	1.56	2.08	3.24
0.9	0.07	0.11	0.28	1.53	2.47	3.77

Table 1: Dependence of the extreme values of I_2/I_1 on the dividing parameter a.

Now, to select the probe geometry (a, R) the most suitable from experimental point of view, the shapes of $I_2/I_1(\beta)$ functions can be assessed in two steps. First, the magnitude of a can selected based on data presented in Tab.1. As the signal sensitivity to flow direction (see the values in the last column) does not change significantly with varying a, as the optimal value of dividing parameter can be selected that giving the same sensitivity for both frontal and reversal flows (compare the values in 4th and 5th column), thus $a = 0.5$ is the best choice. Then, the optimal value of parameter R can be determined from an additional requirement that $I_2/I_1(\beta)$ function should be getting closer to linear one. As seen in Figure 10, this requirement is best fulfilled somewhere on the interval $R \in \langle 1, 2\rangle$. The optimization procedure based on root-mean-square minimization then provides the value $R = 1.54$. Thus, the geometry with $a = 0.5$ and $R = 1.54$ can be suggested as the optimal for experimental measurements with the two strip probe. The comparison of $I_2/I_1(\beta)$ function obtained by

parameter optimization (solid line) with the linear type of dependence (dashed line) is presented in Figure 11.

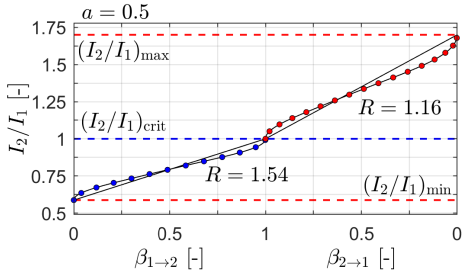

Figure 11: Dependence of I_2/I_1 on the dimensionless flow direction β obtained for the optimal probe geometry ($a = 0.5$ and $R = 1.54$)

On the other hand, the probe with $a = 0.5$ and $R \to 0$ will be suitable for rapid detection of reattachment points, i.e., the locations where the same probability (50 %) is expected for the frontal and reversal flow direction.

4. Conclusions

This paper aims to derive a fundamental theory for describing mass transport on the active surface of a two-strip mass transfer probe for an arbitrary fluid flow direction. The existence and finding of such a general theory is a critical point for using the electrodiffusion method to measure both the magnitude of the shear rate vector and the flow direction by employing two-strip probes. This work follows our previous publication [1], in which we revisited the electro-diffusional theory for the wall shear stress measurement from single mass transfer probes of rectangular shape by considering the existence of two components of the wall shear rate (i.e., longitudinal and transversal). In the present paper, the published theory is generalized to the two-strip probes. The two-dimensional simple shear flow flowing under an arbitrary angle β over the probe of rectangular shape with any aspect ratio R and with different segment lengths was considered. In theory derivation, it was introduced that an idealization assumption that even though the measuring probes are in direct contact,

they are electrically isolated. Based on the introduced conditions, the general analytical formulas were derived for the dimensionless mass transfer coefficients of the front and rear segments. These expressions consider the interactions of the adjacent measuring segments by creating a concentration wake on the front segment. The correctness of the derived analytical expressions for the average nondimensional mass transfer coefficients of the two-segmented probe was confirmed by numerical solutions of the non-dimensional convection-diffusion transport equation. Also, a methodology of possible measured data treatment was proposed based on the evaluation of two electric current signals collected from two segments of a two-strip probe. From the derived equations, it is possible to determine the magnitude and direction of the wall shear rate from the measured data for both frontal and reversal flow. Established on the analysis of the current ratios predictions for various probe geometries was found out an optimal probe configuration concerning the sensitivity of flow direction measurement. It was found that the aspect ratio $R = 1.54$ and the dividing coefficient value is $a = 0.5$ are ideal for determining the fluid flow direction. On the other hand, the probe with $a = 0.5$ and $R \to 0$ will be suitable for rapidly detecting reattachment points. From our research and theory, the possibility opens up to apply a two-strip probe not only for flow reversal detection but also to determine the actual flow direction.

5. Acknowledgments

The authors thank the Research Programme Strategy AV21 Water for life for valuable support. Jaromir Havlica and Vaclav Harrandt acknowledge the support of this work by the Internal Grant Agency of Jan Evangelista Purkyně University in Ústí nad Labem (project no. UJEP-SGS-2020-53-003-3). This project was funded with state support from the Technology Agency of the Czech Republic under the THETA Programme (project No. TK02030155).

Appendix A. Average mass transfer coefficient

One of the ways to determine the average mass transfer coefficient is to use the knowledge of the concentration field near the active surface of the probe. In the case of a perpendicular fluid flow across the leading edge of the probe, mass transport is described by a partial differential equation (14) with boundary conditions (15). By solving this equation with boundary conditions, the following dependence for concentration can be obtained

$$\frac{c - c_{\mathrm{w}}}{c_{\infty} - c_{\mathrm{w}}} = \frac{1}{\Gamma(\frac{4}{3})} \int_0^{\eta} e^{-\eta^3} \mathrm{d}\eta \,, \tag{A.1}$$

where

$$\eta = z \left(\frac{S_x}{9xD} \right)^{\frac{1}{3}} . \tag{A.2}$$

By solving the integral in the equation (A.1) and then substituting for variable η, Eq. (A.1) is changed to shape

$$\frac{c - c_{\mathrm{w}}}{c_{\infty} - c_{\mathrm{w}}} = \frac{1}{\Gamma\left(\frac{4}{3}\right)} \left(\Gamma\left(\frac{4}{3}\right) - \frac{1}{3} \left[z \left(\frac{S_x}{9xD} \right)^{\frac{1}{3}} E_{\frac{2}{3}} \left(z^3 \left(\frac{S_x}{9xD} \right) \right) \right] \right) , \tag{A.3}$$

where E denotes the exponential integral. To calculate the average mass transfer coefficient, knowledge of the derivative of the concentration in the normal direction to the electrode surface is required

$$\frac{\partial c}{\partial z} = \frac{c_{\infty} - c_{\mathrm{w}}}{\Gamma\left(\frac{4}{3}\right)} \left[z^3 \left(\frac{S_x}{9xD} \right)^{\frac{4}{3}} E_{-\frac{1}{3}} \left(z^3 \left(\frac{S_x}{9xD} \right) \right) - \frac{1}{3} \left(\frac{S_x}{9xD} \right)^{\frac{1}{3}} E_{\frac{2}{3}} \left(z^3 \left(\frac{S_x}{9xD} \right) \right) \right] . \tag{A.4}$$

It is important to know the concentration's derivative directly on the probe's active surface to calculate the average mass transfer coefficient. For this reason, the equation (A.4) must be adjusted to the form

$$\lim_{z \to 0} \left(\frac{\partial c}{\partial z} \right) = \frac{c_{\infty} - c_{\mathrm{w}}}{\Gamma(\frac{4}{3})} \left(\frac{S_x}{9xD} \right)^{\frac{1}{3}} . \tag{A.5}$$

For the average mass transfer coefficient, the following equation applies to the perpendicular flow of liquid across the leading edge of the probe

$$\overline{k}_z = \frac{1}{(c_{\infty} - c_{\mathrm{w}}) L_x} \int_0^{L_x} \left(D \frac{\partial c}{\partial z} \right)_{z=0} \mathrm{d}x \,. \tag{A.6}$$

By substituting the equation (A.5) into the equation (A.6) and subsequent modification, the formula is obtained

$$\overline{k}_z = \frac{1}{L_x \Gamma(\frac{4}{3})} \left(\frac{D^2 S_x}{9} \right)^{\frac{1}{3}} \int_0^{L_x} x^{-\frac{1}{3}} \mathrm{d}x \,. \tag{A.7}$$

The last step is the integration and filling of the integral limits. Eq. (A.7) is turned into a generally known relation

$$\overline{k}_z = \frac{3}{2\Gamma(\frac{4}{3}) 9^{\frac{1}{3}}} \left(\frac{D^2 S_x}{L_x} \right)^{\frac{1}{3}} \doteq 0.807549 \left(\frac{D^2 S_x}{L_x} \right)^{\frac{1}{3}} . \tag{A.8}$$

References

[1] J. Havlica, D. Kramolis, F. Huchet, A revisit of the electro-diffusional theory for the wall shear stress measurement, International Journal of Heat and Mass Transfer (2021). doi:https://doi.org/10.1016/j.ijheatmasstransfer.2020.120610.

[2] F. Huchet, P. Legentilhomme, J. Legrand, A. Montillet, J. Comiti, Unsteady flows in milli- and microsystems: analysis of wall shear rate fluctuations., Experiments in Fluids 51 (2011) 597–610. doi:10.1007/s00348-011-1079-1.

[3] M. Altheimer, D. Becker, F. P. D'Aleo, P. R. von Rohr, Flow regime and liquid solid mass transfer investigation in a designed porous structure using electrochemical micro-probes., Chemical Engineering Science 152 (2016) 699–708. doi:10.1016/j.ces.2016.06.066.

[4] D. Nemec, J. Levec, Flow through packed bed reactors: 1. single-phase flow, Chemical Engineering Science 60 (24) (2005) 6947–6957. doi:https://doi.org/10.1016/j.ces.2005.05.068.

[5] S. S. Bu, J. Yang, Q. T. Dong, Q. W. Wang, Experimental study of flow transitions in structured packed beds of spheres with electrochemical technique., Experimental Thermal and Fluid Science 60 (2015) 106–114. doi:10.1016/j.expthermflusci.2014.09.001.

[6] T. M. Squires, S. R. Quake, Microfluidics: Fluid physics at the nanoliter scale, Reviews of modern physics 77 (2005) 977–1026. doi:10.1103/RevModPhys.77.977.

[7] F. Huchet, J. Havlica, P. Legentilhomme, A. Montillet, J. Comiti, J. Tihon, Use of electrochemical microsensors for hydrodynamics study in crossing microchannels., Microfluidics and Nanofluidics 5 (2008) 55–64. doi:10.1007/s10404-007-0220-1.

[8] P. Panuska, Z. Nejedla, J. Smejkal, P. Aubrecht, M. Liegertova, M. Stofik, J. Havlica, J. Maly, A millifluidic chip for cultivation of fish embryos and toxicity testing fabricated by 3d printing technology, RSC Advances 11 (2021) 20507–20518. doi:10.1039/d1ra00846c.

[9] T. Mizushina, The electrochemical method in transport phenomena, Advances in Heat Transfer 7 (1971) 87–161. doi:10.1016/S0065-2717(08)70017-0.

[10] N. A. Mouheb, A. Montillet, C. Solliec, J. Havlica, P. Legentilhomme, J. Comiti, J. Tihon, Flow characterization in t-shaped and cross-shaped micromixers., Microfluidics and Nanofluidics 10 (2011) 1185–1197. doi:10.1007/s10404-010-0746-5.

[11] J.-L. Zhang, W.-F. Li, X.-L. Xu, L. H.-F., W. F.-Ch., Experimental investigation of three-dimensional flow regimes in a cross-shaped reactor, Physics of Fluids 31 (2019) 034105. doi:10.1063/1.5080501.

[12] J. Tihon, Application of the electrodiffusion method for near-wall flow diagnostics, EFM13 - EXPERIMENTAL FLUID MECHANICS 2013 67 (2014). doi:10.1051/epjconf/20146702117.

[13] L. P. Reiss, T. J. Hanratty, Measurement of instantaneous rates of mass transfer to a small sink on a wall, AIChE Journal 8 (1962) 245–247. doi:https://doi.org/10.1002/aic.690080223.

URL https://aiche.onlinelibrary.wiley.com/doi/abs/10.1002/aic.690080223

[14] L. P. Reiss, T. J. Hanratty, An experimental study of the unsteady nature of the viscous sublayer., Aiche Journal 9 (2) (1963) 154–160. doi:10.1002/Aic.690090204.

[15] T. J. Hanratty, J. A. Campbell, Measurement of wall shear stress., Taylor&Francis, 1983.

[16] J. R. Selman, C. W. Tobias, Mass-transfer measurements by the limiting-current technique, Advances in Chemical Engineering 10 (1978) 211–318.

[17] T. J. Hanratty, Use of the polarographic method to measure wall shear-stress, Journal of applied electrochemistry 21 (1991) 1038–1046. doi:10.1007/BF01041444.

[18] L. Böhm, S. Jankhah, J. Tihon, P. R. Bérubé, M. Kraume, Application of the electrodiffusion method to measure wall shear stress: integrating theory and practice, Chemical Engineering & Technology 37 (2014) 1–14. doi:https://doi.org/10.1002/ceat.201400026.

[19] C. Thobie, W. Blel, J.-L. Hauser, J. Pruvost, C. Gentric, Different types of bubbly flows in a confined channel with the aim of limiting microalgae biofilm development - part i: Hydrodynamic study, Chemical Engineering and Processing - Process Intensification 173 (2022) 108844. doi:10.1016/j.cep.2022.108899.

[20] J. S. Son, T. J. Hanratty, Velocity gradients at the wall for flow around a cylinder at reynolds numbers from 5×10^3 to 10^5, Journal of Fluid Mechanics 35 (2) (1969) 353–368. doi:10.1017/S0022112069001157.

[21] J. Tihon, V. Tovchigrechko, V. Sobolik, O. Wein, Electrodiffusion detection of the near-wall flow reversal in liquid films at the regime of solitary waves., Journal of Applied Electrochemistry 33 (2003) 577–587. doi:10.1023/A:1024988602276.

[22] M. Zhuoxiong, T. J. Hanratty, Analysis of wall shear stress probes in large amplitude unsteady flows, International Journal of Heat and Mass Transfer 34 (1) (1991) 281–290. doi:https://doi.org/10.1016/0017-9310(91)90194-J.

[23] Z. Mao, T. J. Hanratty, Application of an inverse mass-transfer method to the measurement of turbulent fluctuations in the velocity-gradient at the wall., Experiments in Fluids 11 (1) (1991) 65–73. doi:10.1007/Bf00198433.

[24] Z. Mao, H. T. J., Measurement of wall shear rate in large amplitude unsteady reversing flows, Experiments in Fluids 12 (1992) 342–350. doi:10.1007/BF00187312.

[25] E. Berrich, F. Aloui, J. Legrand, Analysis of inverse method applied on sandwich probes, Journal of Fluids Engineering 135 (1) (2012). doi:10.1115/1.4007888.

[26] C. Tournier, B. Py, The behaviour of naturally oscillating three-dimensional flow around a cylinder, Journal of fluid mechanics 85 (1978) 161–186. doi:10.1017/S0022112078000579.

[27] J. Tihon, V. Penkavova, J. Havlica, M. Simcik, The transitional backward-facing step flow in a water channel with variable expansion geometry., Experimental Thermal and Fluid Science 40 (2012) 112–125. doi:10.1016/j.expthermflusci.2012.02.006.

[28] V. E. Nakoryakov, O. N. Kashinsky, B. K. Kozmenko, Experimental study of gas-liquid slug flow in a small-diameter vertical pipe, International journal of multiphase flow 12 (1986) 337–355. doi:10.1016/0301-9322(86)90012-1.

[29] K. Ezeji, J. Tihon, Near-wall flow response to large air bubbles rising in inclined water channels, Chemical engineering science 24 (2022). doi:10.1016/j.ces.2021.116914.

[30] M. Gradeck, M. LeBouche, Wall shear measurements inside corrugated channels using the electrochemical technique, Experiments in Fluids 13 (1998) 17–26. doi:10.1007/s003480050146.

[31] G. Cognet, M. LeBouche, M. Souhar, Wall shear measurements by electrochemical probe for gas-liquid two-phase flow in vertical duct, AIChE Journal 30 (1984) 338–341. doi:10.1002/aic.690300224.

[32] O. Wein, V. Sobolík, Theory of direction sensitive probes for electrodiffusion measurement of wall velocity gradients, Collection of Czechoslovak chemical communications 52 (9) (1987) 2169–2180. doi:https://doi.org/10.1135/cccc19872169.

[33] M. E. Lamarche-Gagnon, J. Vetel, An inverse problem to assess the two-component unsteady wall shear rate., International Journal of Thermal Sciences 130 (2018) 278–288. doi:10.1016/j.ijthermalsci.2018.04.022.

[34] J. Tihon, V. Pěnkavová, J. Vejražka, Wall shear stress induced by a large bubble rising in an inclined rectangular channel, International Journal of Multiphase Flow 67 (2014) 76–87. doi:https://doi.org/10.1016/j.ijmultiphaseflow.2014.07.005.

[35] V. Sobolik, J. Tihon, O. Wein, K. Wichterle, Calibration of electrodiffusion friction probes using a voltage-step transient, Journal of Applied Electrochemistry 28 (1998) 329–335. doi:10.1023/A:1003224018571.

[36] M. LeBouche, Polarographic measurement of parietal velocity-gradient in zones of arrest upstream or of separation of cylinders, Comptes Rendus Hebdomadaires Des Seances De L Academie Des Sciences Serie A 276 (1973) 1245–1248.

[37] B. Py, 3-dimensional study of viscous sublayer in a channel flow by mass-transfer measurements, International Journal of Heat and Mass Transfer 16 (1973) 129–144. doi:10.1016/0017-9310(73)90257-3.

[38] O. Wein, K. Wichterle, Theory of segmented electrodiffusion probes: The effect of insulating insertions, Collection of Czechoslovak chemical communications 54 (1989) 3198–3212. doi:10.1135/cccc19893198.

[39] E. Guyon, J.-P. Hulin, L. Petit, C. D. Mitescu, Physical Hydrodynamics, Oxford University Press, 2015.

List of used symbols:

a	splitting coefficient	[-]
c	concentration	$[\mathrm{mol\,m^{-3}}]$
D	diffusivity of mass	$[\mathrm{m^2\,s^{-1}}]$
E	exponential integral	
f	auxiliary function	
F	Faraday constant	$[\mathrm{C\,mol^{-1}}]$
g	auxiliary function	
I	electric current	[A]
J	molar flux intensity	$[\mathrm{mol\,m^{-2}\,s^{-1}}]$
k	mass transfer coefficient	$[\mathrm{m\,s^{-1}}]$
K	auxiliary constant defined by equation (79)	$[\mathrm{m\,s^{-1}}]$
K_{L}	Lévêque constant $(\frac{3}{2\Gamma(\frac{4}{3})9^{\frac{1}{3}}})$	[-]
l	length of individual strip segment	[m]
$\mathrm{d}v$	infinitesimal width of the strip segment	[m]
l_D	characteristic length	[m]
l_{e}	effective transfer length	[m]
L_x	longitudinal dimension of probe	[m]
L_y	transverse dimension of probe	[m]
n_{e}	number of electrons involved in redox reaction	[-]
$\mathbf{n}$	normal vector	[-]
R	aspect ratio of sides of probes	[-]
S	surface	$[\mathrm{m^2}]$
S_{e}	active surface of the electrode	$[\mathrm{m^2}]$
$\mathbf{S}$	wall shear rate vector	$[\mathrm{s^{-1}}]$
Sc	Schmidt number	[-]
$Sh^*_{l_D}$	normalized Sherwood number for a given characteristic length	[-]
Pe	Peclet number	[-]
t	time	[s]

$\mathbf{u}$	velocity field vector	$[\mathrm{m\,s^{-1}}]$
x, y, z	cartesian coordinates	[m]
α	angle at which liquid is flowing on the electrode	[-]
β	dimensionless angle at which liquid is flowing on the electrode	[-]
β_c	critical value of dimensionless angle	[-]
Γ	gamma function	
δ_{D,l_D}	thickness of diffusion boundary layer for a given characteristic length l_D	[m]
η	variable defined by equation (17)	[-]
μ	dynamic viscosity	[Pa s]
ν	kinematic viscosity	$[\mathrm{m^2\,s^{-1}}]$
τ_w	magnitude of wall shear stress	[Pa]

List of subscripts:

1	quantities related to the front electrode of sandwich arrangement
2	quantities related to the rear electrode of sandwich arrangement
$1 \to 2$	direction of liquid in frontal flow direction
$2 \to 1$	direction of liquid in reversal flow direction
∞	bulk
lim	limiting value
w	equilibrium value on the probe surface
z	in the z axis direction

List of superscripts:

+	dimensionless quantity
R	quantities related to the reversal flow direction